Conserving GW scheme for nonequilibrium quantum transport in molecular contacts

Thygesen, Kristian Sommer; Rubio, Angel

Published in:
Physical Review B (Condensed Matter and Materials Physics)

Link to article, DOI:
10.1103/PhysRevB.77.115333

Publication date:
2008

Document Version
Publisher's PDF, also known as Version of record

Conserving *GW* scheme for nonequilibrium quantum transport in molecular contacts

Kristian S. Thygesen[1] and Angel Rubio[2]
[1]*Center for Atomic-scale Materials Design (CAMD), Department of Physics, Technical University of Denmark, DK-2800 Kgs. Lyngby, Denmark*
[2]*European Theoretical Spectroscopy Facility (ETSF), Departamento de Física de Materiales, Edificio Korta, Universidad del País Vasco, Centro Mixto CSIC-UPV, and Donostia International Physics Center (DIPC), Avenida de Tolosa 71, E-20018 Donostia-San Sebastián, Spain*

(Received 11 September 2007; revised manuscript received 14 January 2008; published 18 March 2008)

We give a detailed presentation of our recent scheme to include correlation effects in molecular transport calculations using the nonequilibrium Keldysh formalism. The scheme is general and can be used with any quasiparticle self-energy, but for practical reasons, we mainly specialize to the so-called *GW* self-energy, widely used to describe the quasiparticle band structures and spectroscopic properties of extended and low-dimensional systems. We restrict the *GW* self-energy to a finite, central region containing the molecule, and we describe the leads by density functional theory (DFT). A minimal basis of maximally localized Wannier functions is applied both in the central *GW* region and the leads. The importance of using a conserving, i.e., fully self-consistent, *GW* self-energy is demonstrated both analytically and numerically. We introduce an effective spin-dependent interaction which automatically reduces self-interaction errors to all orders in the interaction. The scheme is applied to the Anderson model in and out of equilibrium. In equilibrium at zero temperature, we find that *GW* describes the Kondo resonance fairly well for intermediate interaction strengths. Out of equilibrium, we demonstrate that the one-shot G_0W_0 approximation can produce severe errors, in particular, at high bias. Finally, we consider a benzene molecule between featureless leads. It is found that the molecule's highest occupied molecular orbital–lowest unoccupied molecular orbital gap as calculated in *GW* is significantly reduced as the coupling to the leads is increased, reflecting the more efficient screening in the strongly coupled junction. For the *I-V* characteristics of the junction, we find that Hartree–Fock (HF) and $G_0W_0[G_{\mathrm{HF}}]$ yield results closer to *GW* than does DFT and $G_0W_0[G_{\mathrm{DFT}}]$. This is explained in terms of self-interaction effects and lifetime reduction due to electron-electron interactions.

DOI: 10.1103/PhysRevB.77.115333 PACS number(s): 73.63.−b, 72.10.−d, 71.10.−w

I. INTRODUCTION

Since the first measurements of electron transport through single molecules were reported in the late 1990s,[1–3] the theoretical interest for quantum transport in nanoscale systems has been rapidly growing. An important driving force behind the scientific developments is the potential use of molecular devices in electronics and sensor applications. On the other hand, it is clear that a successful introduction of these technologies is heavily dependent on the availability of theoretical and numerical tools for the accurate description of such molecular devices.

So far, the combination of density functional theory (DFT) and nonequilibrium Green's functions (NEGF) has been the most popular method for modeling nanoscale conductivity.[4–7] For strongly coupled systems such as metallic point contacts, monatomic chains, and contacts with small chemisorbed molecules, this combination has been remarkably successful,[8–10] but in the opposite limit of weakly coupled systems where the conductance is much smaller than the conductance quantum, $G_0=2e^2/h$, the NEGF-DFT method has been found to overestimate the conductance relative to experiments.[11–13] Part of this discrepancy might result from the use of inappropriate exchange-correlation (xc) functionals.[14] However, it is important to remember that the application of ground state DFT to nonequilibrium transport cannot be rigorously justified—even with the exact xc functional. In particular, a breakdown of the effective single-particle DFT description is expected when correlation effects are important or when the system is driven out of equilibrium.

Over the years, several different schemes have been proposed as alternatives to NEGF-DFT. Historically, the first DFT based transport methods used an equivalent formulation in terms of scattering states rather than Green's functions.[15–17] A more recent approach (still within DFT) solves a master equation for the density matrix of an electron system exposed to a constant electric field and coupled to a damping heat bath of auxiliary phonons.[18]

A few attempts have been made to calculate the current in the presence of electronic correlations. In one approach, the density matrix is obtained from a many-body wave function and the nonequilibrium boundary conditions are invoked by fixing the occupation numbers of left- and right-going states.[19] Exact diagonalization within the molecular subspace has been combined with rate equations to calculate tunneling currents to first order in the lead-molecule coupling strength.[20] The linear response conductance of jellium quantum point contacts has been addressed on the basis of the Kubo formula.[21,22] Although this method is restricted to the low bias regime, it has the advantage over the NEGF method that interactions outside the device region can be naturally included. The time-dependent version of density functional theory has also been used as framework for quantum transport.[23–25] This scheme is particularly useful for simulating transients and high frequency ac responses. Within the NEGF formalism, the many-body *GW* approxi-

mation has been used to address correlated transport both under equilibrium[26] and nonequilibrium[27] conditions.

Within the framework of many-body perturbation theory, electronic correlations are described by a self-energy which in practice must be obtained according to some approximate scheme, e.g., by summing a restricted set of Feynman diagrams. The important question then arises whether the quantities calculated from the resulting Green's function will obey the simple conservation laws. In the context of quantum transport, the continuity equation, which ensures charge conservation, is obviously of special interest. An elegant way of invoking the conservation laws is to write the self-energy as the functional derivative of a so-called Φ functional, i.e., $\Sigma[G]=\delta\Phi[G]/\delta G$. Since the self-energy in this way becomes dependent on the Green's function (GF), it must be determined self-consistently in conjunction with the Dyson equation.[28]

Due to the large computational demands connected with the self-consistent solution of the Dyson equation, practical *GW* band structure calculations usually evaluate the self-energy at some approximate noninteracting G_0. This non-self-consistent scheme does not constitute a conserving approximation. While this might not be important for the calculated spectrum, self-consistency has been demonstrated to be fundamental for out-of-equilibrium transport.[27] In addition to its conserving nature, another nice feature of the self-consistent approach is that it leads to a unique GF and, thus, removes the G_0 dependence inherent in the non-self-consistent approach.

A reliable description of electron transport through a molecular junction requires, first of all, a reliable description of the *internal* electronic structure of the molecule itself, i.e., its electron addition and removal energies. The *GW* approximation has been widely and successfully used to calculate such quasiparticle excitations in both semiconductors, insulators, and molecules,[29–33] and on this basis, it seems natural to extend its use to transport calculations.

There are two main obstacles related to the extension of the *GW* method to charge transport. First, the conventional application of the *GW* method has been on ground state problems, whereas transport is an inherent nonequilibrium problem. Second, it is not obvious how to treat electron-electron interactions in the leads within the NEGF formalism. In Ref. 27, we proposed to overcome these problems by extending the *GW* self-energy to the Keldysh contour and by restricting it to a finite central region where correlation effects are expected to be most important. In the present paper, we provide an extended presentation of these ideas.

When a molecule is brought into contact with electrodes, a number of physical mechanisms will affect its electronic structure. Some of these mechanisms are single particle in nature and are already well described at the DFT Kohn–Sham level, but there are also important many-body effects which require a dynamical treatment of the electronic interactions. One example is the renormalization of the highest occupied molecular orbital–lowest unoccupied molecular orbital (HOMO-LUMO) gap induced by the image charges formed in the electrodes when an electron is added to or removed from the molecule.[29,34] Another example is the Kondo effect which results from correlations between a localized spin on the molecule and delocalized electrons in the electrodes.[35,36] Third, as we will show here, the coupling to (noninteracting) electrodes enhances the screening on the molecule leading to characteristic reduction of the HOMO-LUMO gap as function of the electrode-molecule coupling strength.

In this paper, we focus on improving the description of quantum transport in molecular junctions by improving the description of the internal electronic structure of the molecule while preserving a nonperturbative treatment of the coupling to leads. We do this within the NEGF formalism by using a self-consistent *GW* self-energy to include xc effects within the molecular subspace which, in turn, is coupled to noninteracting leads. The rationale behind this division is that the transport properties, to a large extent, are determined by the narrowest part of the conductor, i.e., the molecule, while the leads mainly serve as particle reservoirs. Strictly speaking, this is correct only when a sufficiently large part of the leads is included in the *GW* region. If the central region is too small, spurious backscattering at the interface between the *GW* and the mean-field regions might affect the calculated conductance. Furthermore, the dynamical formation of image charges in the electrodes requires that part of the electrodes are included in the *GW* region. In the present work, however, we do not attempt to address this latter effect.

The paper is organized as follows. In Sec. II, we introduce the model used to describe the transport problem and review the basic elements of the Keldysh Green's function formalism. In Sec. III, we introduce an effective interaction, discuss the problem of self-interaction correction in diagrammatic expansions, and derive the nonequilibrium *GW* equations for an interacting region coupled to noninteracting leads. In Sec. IV, we introduce the current formula and show that charge conservation is fulfilled within the NEGF formalism for Φ derivable self-energies—also when incomplete basis sets are used. The practical implementation of the *GW* transport scheme using a Wannier function basis obtained from DFT is described in Sec. V. In Secs. VI and VII, we present the results for the nonequilibrium transport properties of the Anderson impurity model and the benzene molecule between jellium leads, respectively. In Sec. VIII, we present our conclusions.

II. GENERAL FORMALISM

In this section, we review the elements of the Keldysh Green's function formalism necessary to deal with the nonequilibrium transport problem. To limit the technical details, we specialize to the case of orthogonal basis sets and refer to Ref. 37 for a generalization to the nonorthogonal case.

A. Model

We consider a quantum conductor consisting of a central region (C) connected to left (L) and right (R) leads (Fig. 1). For times $t<t_0$, the three regions are decoupled from each other, each being in thermal equilibrium with a common temperature T and chemical potentials μ_L, μ_C, and μ_R, respectively. At $t=t_0$, the coupling between the three sub-

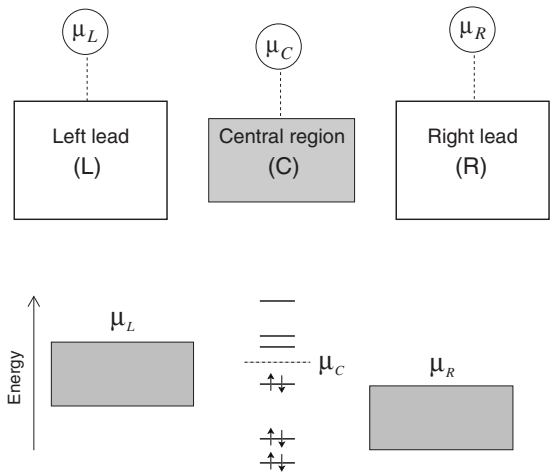

FIG. 1. Before the coupling between the three regions is established, the three subsystems are in equilibrium with chemical potentials μ_L, μ_C, and μ_R, respectively.

systems is switched on and a current starts to flow as the electrode with higher chemical potential discharges through the central region into the lead with lower chemical potential. Our aim is to calculate the steady state current which arise after the transient has died out.

We denote by $\{\phi_i\}$ an orthonormal set of single-particle orbitals and by $\mathcal{H}$ the Hilbert space spanned by $\{\phi_i\}$. The orbitals ϕ_i are assumed to be localized such that $\mathcal{H}$ can be decomposed into a sum of orthogonal subspaces corresponding to the division of the system into leads and central region, i.e., $\mathcal{H}=\mathcal{H}_L+\mathcal{H}_C+\mathcal{H}_R$. We will use the notation $i \in \alpha$ to indicate that $\phi_i \in \mathcal{H}_\alpha$ for some $\alpha \in \{L,C,R\}$.

The noninteracting part of the Hamiltonian of the *connected* system is written

$$\hat{h} = \sum_{\substack{i,j \in \\ L,C,R}} \sum_{\sigma=\uparrow\downarrow} h_{ij} c_{i\sigma}^\dagger c_{j\sigma}, \tag{1}$$

where i,j run over all basis states of the system. For $\alpha,\beta \in \{L,C,R\}$, the operator $\hat{h}_{\alpha\beta}$ is obtained by restricting i to region α, and j to region β in Eq. (1). Occasionally, we shall write $\hat{h}_\alpha$ instead of $\hat{h}_{\alpha\alpha}$. We assume that there is no direct coupling between the two leads, i.e., $\hat{h}_{LR}=\hat{h}_{RL}=0$ (this condition can always be fulfilled by increasing the size of the central region since the basis functions are localized). We introduce a special notation for the "diagonal" of $\hat{h}$,

$$\hat{h}_0 = \hat{h}_{LL} + \hat{h}_{CC} + \hat{h}_{RR}. \tag{2}$$

It is instructive to note that $\hat{h}_0$ does *not* describe the three regions in isolation from each other, but rather the contacted system without inter-region hopping. We allow for interactions between electrons inside the central region. The most general form of such a two-body interaction is

$$\hat{V} = \sum_{\substack{ijkl \in C \\ \sigma\sigma'}} V_{ij,kl} c_{i\sigma}^\dagger c_{j\sigma'}^\dagger c_{l\sigma'} c_{k\sigma}. \tag{3}$$

The full Hamiltonian describing the system at time t can then be written

$$\hat{H}(t) = \begin{cases} \hat{H}_0 = \hat{h}_0 + \hat{V} & \text{for } t < t_0 \\ \hat{H} = \hat{h} + \hat{V} & \text{for } t > t_0. \end{cases} \tag{4}$$

Notice that we use small letters for noninteracting quantities and the subscript 0 for uncoupled quantities. The specific form of the matrix elements h_{ij} and $V_{ij,kl}$ defining the Hamiltonian is considered in Sec. V.

Having defined the Hamiltonian, we now consider the initial state of the system, i.e., the state at times $t<t_0$. For such times, the three subsystems are each in thermal equilibrium and, thus, characterized by their equilibrium density matrices. For the left lead, we have

$$\hat{\varrho}_L = \frac{1}{Z_L} \exp[-\beta(\hat{h}_L - \mu_L \hat{N}_L)] \tag{5}$$

with

$$Z_L = \mathrm{Tr}\{\exp[-\beta(\hat{h}_L - \mu_L \hat{N}_L)]\}. \tag{6}$$

Here, β is the inverse temperature and $\hat{N}_L=\Sigma_{\sigma,i\in L} c_{i\sigma}^\dagger c_{i\sigma}$ is the number operator of lead L. $\hat{\varrho}_R$ and Z_R are obtained by replacing L by R. For $\hat{\varrho}_C$ and Z_C, we must add $\hat{V}$ to account for correlations in the initial state of the central region. The initial state of the whole system is then given by

$$\hat{\varrho} = \hat{\varrho}_L \hat{\varrho}_C \hat{\varrho}_R. \tag{7}$$

If $\hat{V}$ is not included in $\hat{\varrho}_C$, we obtain the uncorrelated (noninteracting) initial state $\hat{\varrho}_{ni}$. We note that the order of the density matrices in Eq. (7) plays no role since they all commute due to the orthogonality of the system $\{\phi_i\}$. Because $\hat{H}_0$ ($\hat{h}_0$) describes the contacted system without inter-region hopping, $\hat{\varrho}$ ($\hat{\varrho}_{ni}$) does not describe the three regions in physical isolation. In other words, the three regions are only decoupled at the *dynamic* level for times $t<t_0$.

B. Contour-ordered Green's function

In this section, we introduce the contour-ordered GF, which is the central object for the many-body perturbation theory in nonequilibrium systems. For more detailed accounts of the NEGF theory, we refer to Refs. 38 and 39.

The contour-ordered GF relevant for the model introduced in the previous section is defined by

$$G_{i\sigma,j\sigma'}(\tau,\tau') = -i\,\mathrm{Tr}\{\hat{\varrho} T[c_{H,i\sigma}(\tau) c_{H,j\sigma'}^\dagger(\tau')]\}. \tag{8}$$

Here, τ and τ' are points on the Keldysh contour, $\mathcal{C}$, which runs along the real-time axis from t_0 to ∞ and back to t_0, and T is the time-ordering operator on the contour. The creation and annihilation operators are taken in the Heisenberg picture with respect to the full Hamiltonian in Eq. (4). We do

not consider spin-flip processes and, thus, suppress the spin indices in the following.

In order to obtain an expansion of $G_{ij}(\tau,\tau')$ in powers of $\hat{V}$, we switch to the interaction picture where we have

$$G_{ij}(\tau,\tau') = -i\,\mathrm{Tr}\left\{\hat{\varrho}T\left[e^{-i\int_{\mathcal{C}}d\bar{\tau}\hat{V}_h(\bar{\tau})}c_{h,i}(\tau)c_{h,j}^{\dagger}(\tau')\right]\right\}. \quad (9)$$

By extending $\mathcal{C}$ into the complex plane by a vertical branch running from t_0 to $t_0-i\beta$, we can replace $\hat{\varrho}$ by the uncorrelated $\hat{\varrho}_{ni}$.[39] Neglecting the vertical branch then corresponds to neglecting correlations in the central region's initial state. While it must be expected that the presence of initial correlations will influence the transient behavior of the current, it seems plausible that they will be washed out over time such that the steady state current will not depend on $\hat{\varrho}_C$. Furthermore, in the special case of equilibrium ($\mu_L=\mu_C=\mu_R$) and zero temperature, the Gellman–Low theorem ensures that the correlations are correctly introduced when starting from the uncorrelated initial state at $t_0=-\infty$.[40] In practice, the neglect of initial correlations is a major simplification which allows us to work entirely on the real axis, avoiding any reference to the imaginary time. For these reasons, we shall adopt this approximation and neglect initial correlations in the rest of this paper.

Equation (9) with $\hat{\varrho}$ replaced by $\hat{\varrho}_{ni}$ constitute the starting point for a systematic series expansion of G_{ij} in powers of $\hat{V}$ and the free propagator,

$$g_{ij}(\tau,\tau') = -i\,\mathrm{Tr}\{\hat{\varrho}_{ni}T[c_{h,i}(\tau)c_{h,j}^{\dagger}(\tau')]\}, \quad (10)$$

which describes the noninteracting electrons in the coupled system. The diagrammatic expansion leads to the identification of a self-energy, Σ, which relates the interacting GF to the noninteracting one through Dyson's equation

$$G(\tau,\tau') = g(\tau,\tau') + \int_{\mathcal{C}} d\tau_1 d\tau_2 g(\tau,\tau_1)\Sigma(\tau_1,\tau_2)G(\tau_2,\tau') \quad (11)$$

(matrix multiplication is implied). As we will see in Sec. IV A, only the Green's function of the central region is needed for the calculation of the current, and we can, therefore, focus on the central-region submatrix of G. Due to the structure of $\hat{V}$, the self-energy matrix Σ_{ij} will be nonzero only when both $i,j\in C$, and for this reason, C subscripts can be added to all matrices in Eq. (11). Having observed this, we will, nevertheless, write Σ instead of Σ_C for notational simplicity.

The free propagator $g_C(\tau,\tau')$, which is still a nonequilibrium GF, satisfies the following Dyson equation:

$$g_C(\tau,\tau') = g_{0,C}(\tau,\tau') + \int_{\mathcal{C}} d\tau_1 d\tau_2 g_{0,C}(\tau,\tau_1)[\Sigma_L(\tau_1,\tau_2) + \Sigma_R(\tau_1,\tau_2)]g_C(\tau_2,\tau'), \quad (12)$$

where g_0 is the *equilibrium* GF defined by $\hat{\varrho}_{ni}$ and $\hat{h}_0$. The coupling self-energy due to lead $\alpha=L,R$ is given by

$$\Sigma_\alpha(\tau,\tau') = h_{C\alpha}g_{0,\alpha}(\tau,\tau')h_{\alpha C}. \quad (13)$$

Notice the slight abuse of notation: Σ_α is *not* the $\alpha\alpha$ submatrix of Σ. In fact, Σ_L and Σ_R are both matrices in the central-region indices. Combining Eqs. (11) and (12), we can write

$$G_C(\tau,\tau') = g_{0,C}(\tau,\tau') + \int_{\mathcal{C}} d\tau_1 d\tau_2 g_{0,C}(\tau,\tau_1)\Sigma_{tot}(\tau_1,\tau_2)G_C(\tau_2,\tau'), \quad (14)$$

which expresses G_C in terms of the equilibrium propagator of the noninteracting, uncoupled system, g_0, and the total self-energy

$$\Sigma_{tot} = \Sigma + \Sigma_L + \Sigma_R. \quad (15)$$

C. Real-time Green's functions

In order to evaluate expectation values of single-particle observables, we need the real-time correlation functions. We work with two correlation functions, also called the lesser and greater GFs and defined as

$$G_{ij}^{<}(t,t') = i\,\mathrm{Tr}\{\hat{\varrho}_{ni}c_{H,j}^{\dagger}(t')c_{H,i}(t)\}, \quad (16)$$

$$G_{ij}^{>}(t,t') = -i\,\mathrm{Tr}\{\hat{\varrho}_{ni}c_{H,i}(t)c_{H,j}^{\dagger}(t')\}. \quad (17)$$

Two other important real-time GFs are the retarded and advanced GFs, defined by

$$G_{ij}^{r}(t,t') = \theta(t-t')[G_{ij}^{>}(t,t') - G_{ij}^{<}(t,t')], \quad (18)$$

$$G_{ij}^{a}(t,t') = \theta(t'-t)[G_{ij}^{<}(t,t') - G_{ij}^{>}(t,t')]. \quad (19)$$

The four GFs are related via

$$G^{>} - G^{<} = G^{r} - G^{a}. \quad (20)$$

The lesser and greater GFs are just special cases of the contour-ordered GF. For example, $G^{<}(t,t')=G(\tau,\tau')$ when $\tau=t$ is on the upper branch of $\mathcal{C}$ and $\tau'=t'$ is on the lower branch. This can be used to derive a set of rules, sometimes referred to as the Langreth rules, for converting expressions involving contour-ordered quantities into equivalent expressions involving real-time quantities. We shall not list the conversion rules here, but refer to Ref. 39 (no initial correlations) or Ref. 38 (including initial correlations). The usual procedure in nonequilibrium is then to derive the relevant equations on the contour using the standard diagrammatic techniques and subsequently convert these equations to real time by means of the Langreth rules. An example of this procedure is given in Sec. III B, where the nonequilibrium GW equations are derived.

1. Equilibrium

In equilibrium, the real-time GFs depend only on the time difference $t'-t$. Fourier transforming with respect to this time difference then brings out the spectral properties of the system. In particular, the spectral function

$$A(\omega) = i[G^r(\omega) - G^a(\omega)] = i[G^>(\omega) - G^<(\omega)] \quad (21)$$

shows peaks at the quasiparticle (QP) energies of the system. In equilibrium, we furthermore have the fluctuation-dissipation theorem,

$$G^<(\omega) = if(\omega - \mu)A(\omega), \quad (22)$$

$$G^>(\omega) = -i(1 - f(\omega - \mu))A(\omega), \quad (23)$$

relating the correlation functions to the spectral function and the Fermi–Dirac distribution function, f. The fluctuation-dissipation theorem follows from the Lehman representation which no longer holds out of equilibrium, and as a consequence, one has to work explicitly with the correlation functions in nonequilibrium situations.

2. Nonequilibrium steady state

We shall work under the assumption that in steady state, all the real-time GFs depend only on the time difference $t' - t$. Taking the limit $t_0 \to -\infty$, this will allow us to use the Fourier transform to turn convolutions in real time into products in frequency space. Applying the Langreth conversion rules to the Dyson equation (14) and Fourier transforming with respect to $t' - t$ then leads to the following expression for the retarded GF of the central region:

$$G_C^r(\omega) = g_{0,C}^r(\omega) + g_{0,C}^r(\omega)\Sigma_{tot}^r(\omega)G_C^r(\omega). \quad (24)$$

This equation can be inverted to yield the closed form

$$G_C^r(\omega) = [(\omega + i\eta)I_C - h_C - \Sigma_L^r(\omega) - \Sigma_R^r(\omega) - \Sigma^r(\omega)]^{-1}. \quad (25)$$

The equation for G^a is obtained by replacing r by a and η by $-\eta$ or, alternatively, from $G^a = (G^r)^\dagger$. For the lesser correlation function, the conversion rules lead to the expression

$$G_C^{</>} = G_C^r\Sigma_{tot}^{</>}G_C^a(\omega) + \Delta^{</>}, \quad (26)$$

where

$$\Delta^{</>} = [I_C + G_C^r\Sigma_{tot}^r]g_{0,C}^{</>}[I_C + \Sigma_{tot}^a G_C^a]. \quad (27)$$

The ω dependence has been suppressed for notational simplicity. Using $\Sigma_{tot}^{r/a} = (g_{0,C}^{r/a})^{-1} - (G_C^{r/a})^{-1}$ together with the equilibrium relations $g_{0,C}^< = -f(\omega - \mu_C)[g_{0,C}^r - g_{0,C}^a]$ and $g_{0,C}^> = -[f(\omega - \mu_C) - 1][g_{0,C}^r - g_{0,C}^a]$, we find

$$\Delta^<(\omega) = 2i\eta f(\omega - \mu_C)G_C^r(\omega)G_C^a(\omega), \quad (28)$$

$$\Delta^>(\omega) = 2i\eta[f(\omega - \mu_C) - 1]G_C^r(\omega)G_C^a(\omega). \quad (29)$$

If the product $G^r(\omega)G^a(\omega)$ is independent of η, we can conclude that $\Delta(\omega) \to 0$ in the relevant limit of small η. However, as explained below, this is not always the case.

3. Bound states and the Δ term

We first focus on noninteracting electrons. In this case, the nonequilibrium correlation functions $g^{</>}$ must be evaluated from Eq. (26) with $\Sigma_{tot} = \Sigma_L + \Sigma_R$. For energies outside the bandwidth of the leads, we have $\Sigma_\alpha^r - \Sigma_\alpha^a = 0$ such that no broadening of the (noninteracting) levels is introduced by the coupling to the leads. At such energies we have $g_C^r - g_C^a = 2i\eta g_C^r g_C^a$, and we conclude from Eqs. (28) and (29) that $\Delta^{</>}$ becomes proportional to the spectral function $A = g_C^r - g_C^a$. Since $A(\omega)$ does not necessarily vanish outside the bandwidth of the leads (it has delta peaks at the position of bound states), it follows that $\Delta^{</>}$ should be included in the calculation of $g^{</>}$ to properly account for the bound states. It is interesting to notice that μ_C, which defines the initial state of the central region, drops out of the equations for g if and only if there are no bound states.

When interactions are present in the central region, correlation effects will reduce the lifetime of any single-particle state in C. Mathematically, this is expressed by the fact that $\Sigma^r - \Sigma^a$ will be nonzero for all physically relevant energies. Consequently, the product $G^r(\omega)G^a(\omega)$ will approach a finite value as $\eta \to 0$, leading to a vanishing $\Delta^{</>}$.

In conclusion, the Δ terms of Eqs. (28) and (29) always vanish when interactions are present in C, while for the noninteracting electrons, they vanish everywhere except for ω corresponding to bound states. We mention that it has recently been shown in the time-dependent NEGF framework that the presence of bound states can affect the long time behavior of the current in the noninteracting case.[41]

III. *GW* EQUATIONS

In this section, we derive and discuss the nonequilibrium *GW* and second-order Born (2B) approximations. However, before addressing the expressions for the self-energies, we introduce an effective interaction which leads to a particularly simple form of the equations and, at the same time, provides a means for reducing self-interaction errors in higher-order diagrammatic expansions.

A. Effective interaction

The direct use of the full interaction Eq. (3) results in a four-index polarization function. The numerical representation and storage of this frequency-dependent four-index function are very demanding, and for this reason, we consider the effective interaction defined by

$$\hat{V}_{\text{eff}} = \sum_{ij,\sigma\sigma'} \tilde{V}_{i\sigma,j\sigma'} c_{i\sigma}^\dagger c_{j\sigma'}^\dagger c_{j\sigma'} c_{i\sigma}, \quad (30)$$

where

$$\tilde{V}_{i\sigma,j\sigma'} = V_{ij,ij} - \delta_{\sigma\sigma'} V_{ij,ji}. \quad (31)$$

This expression follows by restricting the sum in the full interaction Eq. (3) to terms of the form $V_{ij,ij} c_{i\sigma}^\dagger c_{j\sigma'}^\dagger c_{j\sigma'} c_{i\sigma}$ and $V_{ij,ji} c_{i\sigma}^\dagger c_{j\sigma}^\dagger c_{j\sigma} c_{i\sigma}$.

The effective interaction is local in orbital space, i.e., it is a two-point function instead of a four-point function and, thus, resembles the real-space representation. Note, however, that in contrast to the real-space representation $\tilde{V}_{i\sigma,j\sigma'}$ is spin dependent. In particular, the self-interactions $\tilde{V}_{i\sigma,i\sigma}$ are zero by construction and, consequently, self-interaction (in the orbital basis) is avoided to all orders in a perturbation expan-

sion in powers of $\tilde{V}$. Since the off-diagonal elements ($i \neq j$) of the exchange integrals $V_{ij,ji}$ are small, one expects that the main effect of the second term in Eq. (31) is to cancel the self-interaction in the first term.

It is not straightforward to anticipate the quality of a *GW* calculation based on the effective interaction (30) as compared to the full interaction (3). Clearly, if we include all Feynman diagrams in Σ, we obtain the exact result when the full interaction (3) is used, while the use of the effective interaction (30) would yield an approximate result. The quality of this approximate result would then depend on the basis set, becoming better the more localized the basis functions and is equal to the exact result in the limit of completely localized delta functions, where only the direct Coulomb integrals $V_{ij,ij}$ will be nonzero.

However, when only a subset of all diagrams are included in Σ, the situation is different: In the GW approximation, only one diagram per order (in $\hat{V}$) is included, and thus cancellation of self-interaction does not occur when the full interaction is used. On the other hand, the effective interaction (31) is self-interaction-free (in the orbital basis) by construction. The situation can be understood by considering the lowest-order case. There are only two first-order diagrams—the Hartree and exchange diagrams—and each cancel the self-interaction in the other. More generally, the presence of self-interaction in an incomplete perturbation expansion can be seen as a violation of identities of the form $\langle \cdot | c^{\dagger}_{k\sigma'} \cdots c_{i\sigma} c_{i\sigma} \cdots c_{j\sigma''} | \cdot \rangle = 0$ when not all Wick contractions are evaluated. Such expectation values will correctly vanish when the effective interaction is used because the prefactor of the $c_{i\sigma}c_{i\sigma}$ operator, $\tilde{V}_{i\sigma,i\sigma}$, is zero. The presence of self-interaction errors in (non-self-consistent) *GW* calculations was recently studied for a hydrogen atom.[42]

In Appendix B, we compare the performance of the effective interaction with exact results for the Hartree and exchange self-energies of a benzene molecule. These first-order results indicate that the accuracy of *GW* calculations based on the effective interaction (30) should be comparable to *GW* calculations based on the full interaction (3). We stress, however, that in practice only the correlation part of the *GW* self-energy (second- and higher-order terms) is evaluated using $\hat{V}_{\text{eff}}$, while the Hartree and exchange self-energies are treated separately at a higher level of accuracy (see Sec. V C).

B. Nonequilibrium *GW* self-energy

It is useful to split the full interaction self-energy into its Hartree and exchange-correlation parts

$$\Sigma(\tau, \tau') = \Sigma_h(\tau, \tau') + \Sigma_{xc}(\tau, \tau'). \tag{32}$$

The Hartree term is local in time and can be written $\Sigma_h(\tau, \tau') = \Sigma_h(\tau)\delta_{\mathcal{C}}(\tau, \tau')$, where $\delta_{\mathcal{C}}$ is a delta function on the Keldysh contour. Within the *GW* approximation, the exchange-correlation term is written as a product of the Green's function G and the screened interaction W, calculated in the random-phase approximation (RPA). With the effective interaction (30), the screened interaction and the polarization are reduced from four- to two-index functions. For notational simplicity, we absorb the spin index into the orbital index, i.e., $(i\sigma) \to i$ (but we do not neglect it). The *GW* equations on the contour then read

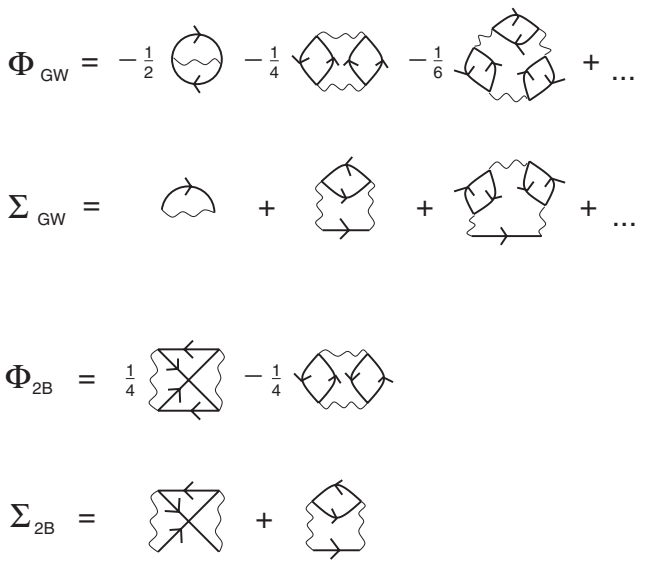

FIG. 2. The *GW* and second Born self-energies, Σ_{GW} and Σ_{2B}, can be obtained as functional derivatives of their respective Φ functionals, $\Phi_{GW}[G]$ and $\Phi_{2B}[G]$. Straight lines represent the full Green's function G, i.e., the Green's function in the presence of coupling to the leads and interactions. Wiggly lines represent the interactions.

$$\Sigma_{GW,ij}(\tau, \tau') = iG_{ij}(\tau, \tau'^{+})W_{ij}(\tau, \tau'), \tag{33}$$

$$W_{ij}(\tau, \tau') = \tilde{V}_{ij}\delta_{\mathcal{C}}(\tau, \tau') + \sum_{kl} \int_{\mathcal{C}} d\tau_1 \tilde{V}_{ik} P_{kl}(\tau, \tau_1) W_{lj}(\tau_1, \tau'), \tag{34}$$

$$P_{ij}(\tau, \tau') = -iG_{ij}(\tau, \tau')G_{ji}(\tau', \tau). \tag{35}$$

It is important to notice that in contrast to the conventional real-space formulation of the *GW* method, the spin dependence cannot be neglected when the effective interaction is used. The reason for this is that $\tilde{V}$ is spin dependent and, consequently, the spin off-diagonal elements of W will influence the spin-diagonal elements of G, Σ, and P. A diagrammatic representation of the *GW* approximation is shown in Fig. 2.

As they stand, Eqs. (33)–(35) involve quantities of the whole system (leads and central region). However, since $\tilde{V}_{ij}$ is nonzero only when $i, j \in C$, it follows from Eq. (34) that W and, hence, Σ also have this structure. Consequently, the subscript C can be directly attached to each quantity in Eqs. (33)–(35); however, for the sake of generality and notational simplicity, we shall not do so at this point. It is, however, important to realize that the GF appearing in the *GW* equations includes the self-energy due to the leads.

Using the Langreth conversion rules,[39] the retarded and lesser *GW* self-energies become (on the time axis)

$$\Sigma^r_{GW,ij}(t) = iG^r_{ij}(t)W^>_{ij}(t) + iG^<_{ij}(t)W^r_{ij}(t), \tag{36}$$

$$\Sigma^{</>}_{GW,ij}(t) = iG^{</>}_{ij}(t)W^{</>}_{ij}(t), \tag{37}$$

where we have used the variable t instead of the time difference $t'-t$. For the screened interaction, we obtain (in frequency space)

$$W^r(\omega) = \tilde{V}[I - P^r(\omega)\tilde{V}]^{-1}, \tag{38}$$

$$W^{</>}(\omega) = W^r(\omega)P^{</>}(\omega)W^a(\omega), \tag{39}$$

where all quantities are matrices in the indices i,σ and matrix multiplication is implied. Notice that the spin off-diagonal part of $\tilde{V}$ will affect the spin-diagonal part of W^r through the matrix inversion.

Finally, the real-time components of the irreducible polarization become

$$P^r_{ij}(t) = -iG^r_{ij}(t)G^<_{ji}(-t) - iG^<_{ij}(t)G^a_{ji}(-t), \tag{40}$$

$$P^{</>}_{ij}(t) = -iG^{</>}_{ij}(t)G^{>/<}_{ji}(-t). \tag{41}$$

From their definitions, it is clear that both the polarization and the screened interaction obey the relations $P^a_{ij}(\omega) = P^r_{ji}(-\omega)$ and $W^a_{ij}(\omega) = W^r_{ji}(-\omega)$, while for the self-energy and GFs, we have $\Sigma^a_{GW}(\omega) = \Sigma^r_{GW}(\omega)^\dagger$ and $G^a(\omega) = G^r(\omega)^\dagger$. In addition, all quantities fulfill the general identity $X^> - X^< = X^r - X^a$. We mention that equations similar to those derived above without the extra complication of coupling to external leads have previously been used to calculate bulk band structures of excited GaAs.[43]

In deriving Eqs. (38) and (39), we have made use of the conversion rules $\delta^{</>}_{\mathcal{C}}(t,t') = 0$ and $\delta^{r/a}_{\mathcal{C}}(t,t') = \delta(t-t')$. With these definitions, the applicability of Langeth rules can be extended to functions containing delta functions on the contour. Notice, however, that with these definitions, relation (18) does not hold for the delta function. The reason why the delta function requires a separate treatment is that the Langreth rules are derived under the assumption that all functions on the contour are well behaved, e.g., do not contain delta functions.

We stress that no spin symmetry has been assumed in the above *GW* equations. Indeed, by reintroducing the spin index, i.e., $i \to (i\sigma)$ and $j \to (j\sigma')$, it is clear that spin-polarized calculations can be performed by treating $G_{\uparrow\uparrow}$ and $G_{\downarrow\downarrow}$ independently.

Within the *GW* approximation, the full interaction self-energy is given by

$$\Sigma(\tau,\tau') = \Sigma_h(\tau,\tau') + \Sigma_{GW}(\tau,\tau'), \tag{42}$$

where the *GW* self-energy can be further split into an exchange part and a correlation part,

$$\Sigma_{GW}(\tau,\tau') = \Sigma_x\delta_{\mathcal{C}}(\tau,\tau') + \Sigma_{\mathrm{corr}}(\tau,\tau'). \tag{43}$$

Due to the static nature of Σ_h and Σ_x, we have

$$\Sigma^{</>}_h = \Sigma^{</>}_x = 0. \tag{44}$$

The retarded components of the Hartree and exchange self-energies become constant in frequency space, and we have [note that for Σ_h and Σ_x we do *not* use the effective interaction (30)]

$$\Sigma^r_{h,ij} = -i\sum_{kl} G^<_{kl}(t=0)V_{ik,jl}, \tag{45}$$

$$\Sigma^r_{x,ij} = i\sum_{kl} G^<_{kl}(t=0)V_{ik,lj}. \tag{46}$$

Due to Eq. (44), it is clear that Eq. (37) yields the lesser and/or greater components of Σ_{corr}. Since $\Sigma_{\mathrm{corr}}(\tau,\tau')$ does not contain delta functions, its retarded component can be obtained from the relation

$$\Sigma^r_{\mathrm{corr}}(t) = \theta(-t)[\Sigma^>_{GW}(t) - \Sigma^<_{GW}(t)]. \tag{47}$$

The separate calculation of Σ^r_x and Σ^r_{corr} from Eqs. (46) and (47), as opposed to calculating their sum directly from Eq. (36), has two advantages: (i) It allows us to treat Σ_x, which is the dominant contribution to Σ_{GW}, at a higher level of accuracy than Σ_{corr} (see Appendix A). (ii) We avoid numerical operations involving G^r and W^r in the time domain (see Appendix E).

C. Nonequilibrium second Born approximation

When screening and/or strong correlation effects are less important, as, e.g., in the case of small molecules, the higher-order terms of the *GW* approximation are small and it is more important to include all second-order diagrams.[33] The full second-order approximation, often referred to as the 2B, is shown diagrammatically in Fig. 2. As we will use the 2B for comparison with the *GW* results, we state the relevant expressions here for completeness. The nonequilibrium 2B has recently been applied to study atoms in laser fields.[44]

On the contour, the 2B self-energy reads [with the effective interaction (30)]

$$\Sigma_{2B,ij}(\tau,\tau') = \sum_{kl} G_{ij}(\tau,\tau')G_{kl}(\tau,\tau')G_{lk}(\tau',\tau)\tilde{V}_{ik}\tilde{V}_{jl} - \sum_{kl} G_{ik}(\tau,\tau')G_{kl}(\tau',\tau)G_{lj}(\tau,\tau')\tilde{V}_{il}\tilde{V}_{jk}. \tag{48}$$

Notice that the first term in Σ_{2B} is simply the second-order term of the *GW* self-energy. From Eq. (48), it is easy to obtain the lesser and/or greater self-energies,

$$\Sigma^{</>}_{2B,ij}(t) = \sum_{kl} G^{</>}_{ij}(t)G^{</>}_{kl}(t)G^{>/<}_{lk}(-t)\tilde{V}_{ik}\tilde{V}_{jl} - \sum_{kl} G^{</>}_{ik}(t)G^{>/<}_{kl}(-t)G^{</>}_{lj}(t)\tilde{V}_{il}\tilde{V}_{jk},$$

where t has been used instead of the time difference $t-t'$. Since these second-order contributions do not contain delta functions of the time variable, we can obtain the retarded self-energy directly from the Kramers–Kronig relation

$$\Sigma^r_{2B}(t) = \theta(-t)[\Sigma^>_{2B}(t) - \Sigma^<_{2B}(t)] \tag{49}$$

(see Appendix E).

IV. CURRENT FORMULA AND CHARGE CONSERVATION

In this section, we address the question of charge conservation in the model introduced in Sec. II A. In particular, we ask under which conditions the current calculated at the left and right sides of the central region are equal, and we show in Sec. IV D that this is fulfilled whenever the self-energy used to describe the interactions is Φ derivable, independent of the applied basis set.

A. Current formula

As shown by Meir and Wingreen,[45] the particle current from lead α into the central region can be expressed as

$$I_\alpha = \int \frac{d\omega}{2\pi} \mathrm{Tr}[\Sigma^<_\alpha(\omega)G^>_C(\omega) - \Sigma^>_\alpha(\omega)G^<_C(\omega)], \tag{50}$$

where matrix multiplication is understood. By writing $I = (I_L - I_R)/2$, one obtains a current expression symmetric in the L, R indices,

$$I = \frac{i}{4\pi} \int \mathrm{Tr}[(\Gamma_L - \Gamma_R)G^<_C + (f_L\Gamma_L - f_R\Gamma_R)(G^r_C - G^a_C)]d\omega, \tag{51}$$

where we have suppressed the ω dependence and introduced the coupling strength of lead α, $\Gamma_\alpha = i[\Sigma^r_\alpha - \Sigma^a_\alpha]$. We note in passing that for noninteracting electrons, the integral has weight only inside the bias window, whereas this is no longer true when interactions are present.

B. Charge conservation

Due to charge conservation, we expect that in steady state $I_L = -I_R = I$, i.e., the current flowing from the left lead to the molecule is the negative of the current flowing from the right lead to the molecule. We derive a condition for this specific form of particle conservation.

From Eq. (50), the difference between the currents at the left and right interfaces, $\Delta I = I_L + I_R$, is given by

$$\Delta I = \int \frac{d\omega}{2\pi} \mathrm{Tr}[(\Sigma^<_L + \Sigma^<_R)G^>_C - (\Sigma^>_L + \Sigma^>_R)G^<_C]. \tag{52}$$

To obtain a condition for $\Delta I = 0$ in terms of Σ, we start by proving the general identity

$$\int \frac{d\omega}{2\pi} \mathrm{Tr}[\Sigma^<_{tot}(\omega)G^>_C(\omega) - \Sigma^>_{tot}(\omega)G^<_C(\omega)] = 0. \tag{53}$$

To prove this, we insert $G^{</>} = G^r_C\Sigma^{</>}_{tot}G^a_C + \Delta^{</>}$ [from Eq. (26)] in the left hand side of Eq. (53). This results in two terms involving $G^r\Sigma^{</>}_{tot}G^a$ and two terms involving $\Delta^{</>}$. The first two terms contribute by

$$\int \frac{d\omega}{2\pi} \mathrm{Tr}[\Sigma^<_{tot}G^r\Sigma^>_{tot}G^a - \Sigma^>_{tot}G^r\Sigma^<_{tot}G^a]. \tag{54}$$

Inserting $\Sigma^>_{tot} = \Sigma^<_{tot} + (G^a)^{-1} - (G^r)^{-1}$ (see Ref. 46) in this expression and using the cyclic invariance of the trace, it is straightforward to show that Eq. (54) vanishes. The two terms involving $\Delta^{</>}$ contribute to the left hand side of Eq. (53) by

$$\int \frac{d\omega}{2\pi} \mathrm{Tr}[\Sigma^<_{tot}(\omega)\Delta^>(\omega) - \Sigma^>_{tot}(\omega)\Delta^<(\omega)]. \tag{55}$$

As discussed in Sec. II C 3, $\Delta^<$ and $\Delta^>$ are always zero when interactions are present. In the case of noninteracting electrons, we have $\Sigma^{</>}_{tot} = \Sigma^{</>}_L + \Sigma^{</>}_R$, which vanishes outside the bandwidth of the leads. On the other hand, $\Delta^{</>}$ is only nonzero at energies corresponding to bound states, i.e., states lying outside the bands, and thus we conclude that the term (55) is always zero.

From Eqs. (52) and (53), it then follows that

$$\Delta I = \int \frac{d\omega}{2\pi} \mathrm{Tr}[\Sigma^<(\omega)G^>_C(\omega) - \Sigma^>(\omega)G^<_C(\omega)]. \tag{56}$$

We notice that without any interactions, particle conservation in the sense $\Delta I = 0$ is trivially fulfilled since $\Sigma = 0$. When interactions are present, particle conservation depends on the specific approximation used for the interaction self-energy Σ.

C. Conserving approximations

A self-energy is called conserving, or Φ derivable, if it can be written as a functional derivative of a so-called Φ functional, $\Sigma[G] = \delta\Phi[G]/\delta G$.[28] Since a Φ-derivable self-energy depends on G, the Dyson equation must be solved self-consistently. The resulting Green's function automatically fulfills all important conservation laws including the continuity equation, which is of major relevance in the context of quantum transport.

The exact $\Phi[G]$ can be obtained by summing over all skeleton diagrams, i.e., closed diagrams with no self-energy insertions, constructed using the full G as propagator. Practical approximations are then obtained by including only a subset of skeleton diagrams. Two examples of such approximations are provided by the GW and second Born Φ functional and associated self-energies, which are illustrated in Fig. 2. Solving the Dyson equation self-consistently with one of these self-energies, thus, defines a conserving approximation in the sense of Baym.

The validity of the conservation laws for Φ-derivable self-energies follows from the invariance of Φ under certain transformations of the Green's function. For example, it follows from the closed diagrammatic structure of Φ that the transformation[28]

$$G(\mathbf{r}\tau, \mathbf{r}'\tau') \to e^{i\Lambda(\mathbf{r}\tau)}G(\mathbf{r}\tau, \mathbf{r}'\tau')e^{-i\Lambda(\mathbf{r}'\tau')}, \tag{57}$$

where Λ is any scalar function, leaves $\Phi[G]$ unchanged. Using the compact notation $(\mathbf{r}_1, \tau_1) = 1$, the change in Φ when the GF is changed by δG can be written as $\delta\Phi = \int d1d2\Sigma(1,2)\delta G(2,1^+) = 0$, where we have used $\Sigma = \delta\Phi[G]/\delta G$. To first order in Λ, we then have

$$\delta\Phi = i\int d1d2\Sigma(1,2)[\Lambda(2)-\Lambda(1)]G(2,1^+)$$

$$= i\int d1d2[\Sigma(1,2)G(2,1^+)-G(1,2^+)\Sigma(2,1)]\Lambda(1).$$

Since this holds for all Λ (by a scaling argument), we conclude that

$$\int d2[\Sigma(1,2)G(2,1^+)-G(1,2^+)\Sigma(2,1)]=0. \quad (58)$$

It can be shown that this condition ensures the validity of the continuity equation (on the contour) at any point in space.[28]

D. Charge conservation from Φ-derivable self-energies

We show that ΔI of Eq. (56) always vanishes when the self-energy is Φ derivable, i.e., the general concept of a conserving approximation carries over to the discrete framework of our transport model.

We start by noting that Eq. (58) holds for *any* pair $G(1,2)$, $\Sigma[G(1,2)]$ provided Σ is of the Φ-derivable form. In particular, Eq. (58) does not assume that the pair G, $\Sigma[G]$ fulfills a Dyson equation. Therefore, by taking any orthonormal, but not necessarily complete set, $\{\phi_i\}$, and writing $G(1,2)=\Sigma_{ij}\phi_i(\mathbf{r}_1)G_{ij}(\tau_1,\tau_2)\phi_j^*(\mathbf{r}_2)$, we get from Eq. (58) after integrating over $\mathbf{r}_1$,

$$\sum_j \int_{\mathcal{C}} d\tau'[\Sigma_{ij}(\tau,\tau')G_{ji}(\tau',\tau^+)-G_{ij}(\tau^-,\tau')\Sigma_{ji}(\tau',\tau)]=0, \quad (59)$$

which in matrix notation takes the form

$$\int_{\mathcal{C}} d\tau' \ \mathrm{Tr}[\Sigma(\tau,\tau')G(\tau',\tau^+)-G(\tau^-,\tau')\Sigma(\tau',\tau)]=0. \quad (60)$$

Here, Σ_{ij} is exactly the self-energy matrix obtained when the diagrams are evaluated using G_{ij} and the $V_{ij,kl}$ from Eq. (3). The left hand side of Eq. (60), which is always zero for a Φ-derivable Σ, can be written as $\mathrm{Tr}[A^<(t,t)]$ when A is given by Eq. (C1), with $B=\Sigma$ and $C=G$. It then follows from the general result (C2) and the condition (56) that current conservation in the sense $I_L=-I_R$ is always obeyed when Σ is Φ derivable.

The above derivation of Eq. (60) relied on *all* the Coulomb matrix elements, V_{ijkl}, that are included in the evaluation of Σ. Thus, the proof does not carry through if a general truncation scheme for the interaction matrix is used. However, in the special case of a truncated interaction of the form (30), i.e., when the interaction is a two-point function, Eq. (60) remains valid. To show this, it is more appropriate to work entirely in the matrix representation and, thus, define $\Phi[G_{ij}(\tau,\tau')]$ as the sum of a set of skeleton diagrams evaluated directly in terms of G_{ij} and $\tilde{V}_{ij}$. With the same argument as used in Eq. (57), it follows that Φ is invariant under the transformation

$$G_{ij}(\tau,\tau') \to e^{i\Lambda_i(\tau)}G_{ij}(\tau,\tau')e^{-i\Lambda_j(\tau')}, \quad (61)$$

where Λ is now a discrete vector. By adapting the arguments following Eq. (57) to the discrete case, we arrive at Eq. (58) with the replacements $\mathbf{r}_1\to i$ and $\mathbf{r}_2\to j$ and with the integral replaced by a discrete sum over j. Summing also over i leads directly to Eq. (60), which is the desired result.

To summarize, we have shown that particle conservation in the sense $I_L=-I_R$ is obeyed whenever a Φ-derivable self-energy is used *and* either (i) all Coulomb matrix elements $V_{ij,kl}$ or (ii) the truncated two-point interaction of Eq. (30) is used to evaluate Σ.

V. IMPLEMENTATION

In this section, we describe the practical implementation of the Wannier-*GW* transport scheme. After a brief sketch of the basic idea of the method, we outline the calculation of the noninteracting Hamiltonian matrix elements and Coulomb integrals in terms of Wannier orbitals. The explicit expression for the Green's function is given in Sec. V D, and in Sec. V F, we describe our implementation of the Pulay mixing scheme for performing self-consistent Green's function calculations. We end the section with a discussion of the present limitations and future improvements of the method.

A. Interactions in the central region

Most first-principles calculations addressing transport in molecular contacts are based on the assumption that the charge carriers (electrons) can be considered as independent particles governed by an effective single-particle Hamiltonian. A popular choice for the effective Hamiltonian is the Kohn–Sham Hamiltonian of DFT,

$$\hat{h}_s = -\frac{1}{2}\nabla^2 + v_{ext}(\mathbf{r}) + v_h(\mathbf{r}) + v_{xc}(\mathbf{r}), \quad (62)$$

where $v_{ext}(\mathbf{r})$ is the external potential from the ions, $v_h(\mathbf{r})$ is the classical Hartree field, and $v_{xc}(\mathbf{r})$ is the exchange-correlation (xc) potential which to some degree includes e-e interaction effect beyond the Hartree level.

In the present method, we rely on the Kohn–Sham (KS) Hamiltonian to describe the metallic electrodes as well as the coupling into the central region, but we replace the local xc potential by a many-body self-energy inside the central region where correlation effects are expected to be most important. Clearly, this division does not treat all parts of the system on the same footing, and one might be concerned that electrons can scatter off the artificial interface defined by the transition region between the mean-field and many-body description and, thus, introduce an artificial "contact resistance." Such unphysical scattering is certainly expected to affect the calculated properties if the transition region is very close to the constriction of the contact. On the other hand, the central region can, at least in principle, be chosen so large that the transition region occurs deep in the electrodes far away from the constriction. In this case, the large number of available conductance channels in the electrodes should ensure that the calculated properties are not dominated by

interface effects and the noninteracting part of the electrodes will mainly serve as particle reservoirs whose precise structure is unimportant. Thus, the assumption of interactions in the central region seems justified in principle although it might be difficult to fully avoid artificial backscattering in practice.

B. Wannier Hamiltonian and Coulomb integrals

In order to make the evaluation and storing of the *GW* self-energy feasible, we use a minimal basis set consisting of maximally localized, partially occupied Wannier functions[47] obtained from the plane-wave pseudopotential code DACAPO.[48] Below we outline how the Hamiltonian is evaluated in the Wannier function (WF) basis, and we refer to Ref. 49 for more details.

The WFs used to describe the leads are obtained from a bulk calculation (or supercell calculation if the leads have finite cross section). We define the *extended central region* ($C2$) as the molecule itself plus a portion of the leads. $C2$ should be so large that it comprises all perturbations in the KS potential arising from the presence of the molecular contact such that a smooth transition from $C2$ into the bulk is ensured. The WFs inside $C2$ are obtained from a DFT calculation with periodic boundary conditions imposed on the supercell containing $C2$. The resulting WFs will inherit the periodicity of the eigenstates; however, due to their localized nature, they can be unambiguously extended into the lead regions. Thanks to the large size of $C2$, hybridization effects between the molecule and the metal leads will automatically be incorporated into the WFs. With the combined set of WFs (lead+$C2$), we can then represent any KS state of the contacted system up to a few electron volts above the Fermi energy.[47]

In practice, the requirement of complete screening means that 3–4 atomic layers of the lead material must be included in $C2$ on both sides of the molecule. While this size of systems can be easily handled within DFT, it may well exceed what is computationally feasible for a many-body treatment such as the *GW* method even with the minimal WF basis. For this reason, we shall allow the central region (C) to consist of a proper subset of the WFs in $C2$, subject to the requirement that there is no direct coupling across it, i.e., $\langle \phi_i | \hat{h}_s | \phi_j \rangle = 0$ for $i \in L$ and $j \in R$, where the left (right) lead by definition is all WFs to the left (right) of C. With this definition of C, the KS potential outside C is not necessarily periodic (this is, however, always the case outside $C2$), and consequently, the calculation of the coupling self-energies becomes somewhat more involved as compared to the usual situation of periodic leads (see discussion in Appendix D). We stress that the transmission function for the noninteracting KS problem is exactly the same whether C or $C2$ is used as the central region as long as there is no direct coupling across region C.

Having constructed the WFs, we calculate the matrix elements of the effective KS Hamiltonian of the *contacted, unbiased* system, $\langle \phi_i | \hat{h}_s | \phi_j \rangle$. To correct for double counting when the *GW* self-energy is added, we also need the matrix elements, $\langle \phi_i | v_{xc} | \phi_j \rangle$, for WFs belonging to the central region.

The matrix elements defining the interaction $\hat{V}$ in Eq. (3) are calculated as the (unscreened) Coulomb integrals

$$V_{ij,kl} = \int \int d\mathbf{r} d\mathbf{r}' \frac{\phi_i(\mathbf{r})^* \phi_j(\mathbf{r}')^* \phi_k(\mathbf{r}) \phi_l(\mathbf{r}')}{|\mathbf{r} - \mathbf{r}'|} \tag{63}$$

for WFs belonging to the central region. The Coulomb integrals are evaluated in Fourier space using neutralizing Gaussian charge distributions to avoid contributions from the periodic images (see Ref. 50).

C. Hartree and exchange

As already mentioned, it is not feasible to include all the interaction matrix elements when evaluating the frequency-dependent part of the many-body self-energy, Σ_{corr}, which is therefore calculated using the effective interaction of Eq. (30).

However, the exchange term, which can be unambiguously separated from the *GW* self-energy, is evaluated from Eq. (46) using all Coulomb elements of the forms $\{\{V_{ij,ij}\},\{V_{ij,ji}\},\{V_{ii,jj}\},\{V_{ii,ij}\}\}$. As shown in Appendix A, this produces results within 5% of the exact values.

The KS Hamiltonian already includes the Hartree potential of the DFT ground state. In a self-consistent, finite-bias *GW* calculation, the relevant Hartree potential will deviate from the DFT Hartree potential due to the finite bias and the fact that the xc potential is replaced by the *GW* self-energy. This correction, which is much smaller than the full Hartree potential, is treated in the same way as the exchange term, i.e., calculated from Eq. (46) with all Coulomb elements of the form $\{\{V_{ij,ij}\},\{V_{ij,ji}\},\{V_{ii,jj}\},\{V_{ii,ij}\}\}$. As for the exchange terms, this yields results within 5% of the exact values (see Appendix A).

D. Expression for G^r

To simplify the notation, in the following we omit the subscript C as all quantities will be matrices in the central region. The retarded GF of the central region is obtained from

$$G^r = \{(\omega + i\eta)I - (h_s - v_{xc}) - \Sigma_L^r - \Sigma_R^r - (\Sigma_h^r[G] - \Sigma_h^r[g_s^{(\mathrm{eq})}]) - \Sigma_{GW}^r[G]\}^{-1}. \tag{64}$$

Several comments are in order. First, we notice that all quantities except for v_{xc}, h_s, and $\Sigma_h^r[g_s^{(\mathrm{eq})}]$ are bias dependent; however, to keep the notation as simple as possible, we omit any reference to this dependence. The terms Σ_L^r and Σ_R^r account for the coupling to the leads. By subtracting v_{xc} from h_s, we ensure that exchange-correlation effects are not counted twice when we add the *GW* self-energy, Σ_{GW}^r. The term $\Delta v_h = \Sigma_h^r[G] - \Sigma_h^r[g_s^{(\mathrm{eq})}]$ is the change in Hartree potential relative to the equilibrium DFT value. This change is due to the applied bias and the replacement of v_{xc} by Σ_{GW}^r (even in equilibrium, the Hartree field will change during the *GW* self-consistency cycle). The Hartree potential in C originating from the electron density in the electrodes, which enters

G^r through h_s, is assumed to stay constant when the system is driven out of equilibrium, i.e., the out-of-equilibrium charge distribution in the leads is assumed to equal the equilibrium one.

Finally, in order to make contact with the general formalism of Sec. II, and in particular Eq. (25), we note that the matrix elements h_{ij} defining the effective single-particle Hamiltonian in Eq. (1) are related to the quantities introduced above via

$$h_{ij} = \begin{cases} \langle \phi_i | \hat{h}_s - \hat{v}_{xc} | \phi_j \rangle - \Sigma_h^r [g_s^{(\mathrm{eq})}]_{ij} & \text{for } i,j \text{ both in } C \\ \langle \phi_i | \hat{h}_s | \phi_j \rangle + (\mu_{L(R)} - \varepsilon_F)\delta_{ij} & \text{for } i,j \text{ both in } L(R) \\ \langle \phi_i | \hat{h}_s | \phi_j \rangle & \text{otherwise.} \end{cases}$$

E. Frequency dependence

To represent the temporal dependence of the Green's functions and *GW* self-energies, we use an equidistant frequency grid with N_g grid points and grid spacing δ. Thus, the GFs (and the *GW* self-energies) are represented by $N_w \times N_w \times N_g$ matrices. At each of the discrete frequencies $\omega_i = n_i\delta$, $n_i = 0, \ldots, N_g$, we have an $N_w \times N_w$ matrix representation of $G(\omega_i)$ in the WF basis. The grid spacing δ should be small enough that all features in the frequency dependence of the GFs and self-energies can be resolved. At the same time, the frequency grid should be large enough (contain enough points) to properly describe the asymptotic behavior (the tail) of the GFs. Although the tail is irrelevant for the current in Eq. (51), it contributes to the self-energy, $\Sigma_{GW}[G]$. In practice, N_g and δ should be increased and decreased, respectively, until the results do not change.

To avoid time consuming convolutions on the frequency grid, we use the fast Fourier transform (FFT) to switch between frequency and time domains. An important but technical issue concerning the evaluation of retarded functions is discussed in Appendix E.

F. Self-consistency

Since Σ depends on G, and G depends on Σ, the Dyson equations (26) and (64) must be solved self-consistently in conjunction with the equations for the *GW*, Hartree, and exchange self-energies. In practice, this self-consistent problem is solved by iteration. Clearly, the iterative approach relies on the assumption that the problem has a unique solution and that the iterative process converges to this solution. For all applications we have studied so far, this has been the case. In order to stabilize the iterative procedure, we use the Pulay scheme[51] to mix the GFs of the previous N iterations, very similar to what is done for the electron density in many DFT codes. More specifically, the input GF at iteration n is obtained according to

$$G_{\mathrm{in}}^{X,n} = (1-\alpha)\sum_{j=n-N}^{n-1} c_j^n G_{\mathrm{in}}^{X,j} + \alpha \sum_{j=n-N}^{n-1} c_j^n G_{\mathrm{out}}^{X,j}, \quad X \le r. \tag{65}$$

To determine the optimal values for the expansion coefficients, c^n, we first define an inner product in the space of (retarded) GFs

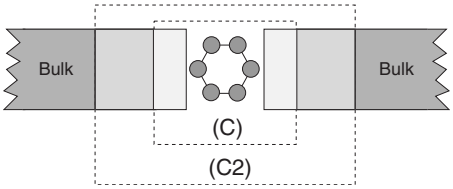

FIG. 3. The extended central region ($C2$) is chosen so large that it comprises all perturbations in the effective DFT potential arising from the molecular contact. The central region (C) can be a proper subregion of $C2$, but it must be so large that there is no direct coupling across it. We solve for the self-consistent Kohn–Sham potential within $C2$, but we replace the static xc potential by the *GW* self-energy inside C.

$$\langle G^{r,i}, G^{r,j} \rangle = \sum_n \int \mathrm{Im}[G_{nn}^{r,i}(\omega)]^* \, \mathrm{Im}[G_{nn}^{r,j}(\omega)] d\omega. \tag{66}$$

Equivalent inner products can be obtained, e.g., by using the real part of the GF instead of the imaginary part or the lesser component instead of the retarded part. The Pulay residue matrix determining the coefficients c^n is then given by

$$A_{ij}^n = \langle G_{\mathrm{in}}^{r,i} - G_{\mathrm{out}}^{r,i}, G_{\mathrm{in}}^{r,j} - G_{\mathrm{out}}^{r,j} \rangle, \tag{67}$$

where $i,j = n-N, \ldots, n-1$. We typically use a mixing factor around $\alpha \approx 0.4$. During the mixing procedure, one must keep track of both the retarded and lesser GFs since one does not follow directly from the other. However, it is important that the *same* coefficients, c^n, are used for mixing the two components. If separate coefficients are used for G^r and $G^<$, the fundamental relation (20) is not guaranteed during the self-consistent cycle. As noted above, we define the residue exclusively from the retarded GF. In practice, we always find that once the retarded GF has converged, the lesser GF has converged too, and this justifies the use of common expansion coefficients for the two GF components.

G. Overview

We give an overview of the various steps involved in performing a self-consistent nonequilibrium *GW* transport calculation as follows:

(1) Perform DFT calculations for the electrodes and the extended central region (region $C2$ in Fig. 3).

(2) Construct the Wannier functions and obtain the matrix representation of the KS Hamiltonian for the contacted system in equilibrium. Evaluate the matrix elements for v_{xc} and relevant Coulomb integrals for Wannier functions belonging to the central region (C).

(3) Fix the bias voltage and calculate the coupling self-energies Eq. (13) as described in Appendix D (these stay unchanged during self-consistency).

(4) Evaluate the initial (noninteracting) Green's functions, G_C^r and $G_C^<$, e.g., from the KS Hamiltonian.

(5) From G_C^r and $G_C^<$, construct the desired interaction self-energies (Σ_h, Σ_x, Σ_{GW}, or Σ_{2B}).

(6) Test for self-consistency. In the negative, obtain a new set of output Green's functions from Eqs. (64) and (26), and

mix with the previous GFs as described in Sec. V F.

H. Limitations and future improvements

The main approximation of the present implementation is the use of a fixed, minimal basis set. We have used WFs obtained from the DFT-PBE orbitals (where PBE denotes Perdew–Burke–Ernzerhof); however, one could also use Hartree–Fock or some other mean-field orbitals. Out of equilibrium, the WFs will be distorted due to the change in electrostatic potential; however, this effect is not included. Although the manifold spanned by the WFs, i.e., the KS eigenstates up to a few electron volts above the Fermi level, are expected to represent the *GW* quasiparticle wave functions of the same energy range quite well, an accurate representation of the screened interaction might require inclusion of high-energy eigenstates.

With the present implementation of the *GW* scheme, it is not feasible to include more than a few electrode atoms in addition to the molecule itself in the *GW* region (region *C* in Fig. 3). The use of a small *C* region might affect the description of image charge formations in the electrode, and it might introduce artificial backscattering at the DFT-*GW* interface.

The use of larger and more accurate basis sets as well as the inclusion of more electrode atoms in the *GW* region are not fundamental but practical limitations of the method, which, in principle, could be removed by invoking efficient simplifications and/or approximations into the present formalism.

VI. ANDERSON MODEL

Since its introduction in 1961, the Anderson impurity model[52] has become a standard tool to investigate strong correlation phenomena such as local moments formation, Kondo effects, and Coulomb blockade. The Anderson model describes a localized electronic level of energy ε_c and correlation energy U coupled to a continuum of states. Thus, the central-region part of the Hamiltonian reads

$$\hat{H}_C = \varepsilon_c c^\dagger c + U n_\uparrow n_\downarrow. \tag{68}$$

In equilibrium, accurate results for the thermodynamic properties of the Anderson model have been obtained from the Bethe ansatz,[53,54] quantum Monte Carlo simulations,[55,56] and numerical renormalization group theory.[36,57]

Out of equilibrium, the low-temperature properties of the Anderson model have been much less studied. The earliest work addressed the problem by applying second-order perturbation theory in the interaction strength U.[58,59] Despite the simplicity of this approach, it provides a surprisingly good description of the (equilibrium) spectral function. There are, however, several fundamental problems related to the nonself-consistent low-order perturbative approach: (i) the result depends on the starting point around which the perturbation is applied, (ii) it inevitably violates the conservation laws, and (iii) it applies only in the small-U limit. Methods relying on the slave-boson technique[60] have been developed to explore the strong correlation regime of the model. The noncrossing approximation is believed to work well in the infinite-U limit and for sufficiently small tunneling strength, Γ, but it fails to reproduce the correct Fermi liquid behavior at low temperatures.[61,62] More recently, a finite-U slave-boson mean-field approach[63] has been proposed. Finally, we mention that a number of more advanced schemes have been used to address nonequilibrium Kondo-like phenomena focusing on the low-energy properties of the Anderson model in the limit where U is much larger than the hybridization energy, Γ.[64–66]

While the Anderson model is normally used to describe strongly correlated systems, the main application of the *GW* approximation has been on weakly interacting quasiparticles in closed shell systems such as molecules, insulators, and semiconductors. In view of this, one could argue that the *GW* method is inappropriate for the Anderson model. Nevertheless, we find this application rather instructive as it illustrates some general features of the *GW* approximation including the role of self-consistency both in relation to charge conservation and the line shape of spectral functions. Moreover, as many important transport phenomena, such as Kondo effects and Coulomb blockade, are well described by the Anderson model, it should always be of interest to benchmark a transport scheme against this model.

In a very recent study,[67] the *GW* approximation was applied to the Anderson model in equilibrium for interaction strengths U/Γ up to $8.4/0.65 \approx 13$ and various temperatures. For the largest interaction strength, it was found that *GW* prefers to break the spin symmetry, leading to directly erroneous results in the Kondo regime. For intermediate interaction strengths ($U/\Gamma = 4.2/0.65 \approx 6.5$) where *GW* does not break the spin symmetry, it was concluded that *GW* does not describe the T dependence of the Kondo effect well. Nevertheless, we show here that at $T=0$, the width of the *GW* Kondo-like resonance follows the analytical result for T_K quite well for intermediate interaction strengths.

Here, as in our previous paper,[27] we focus on the zero temperature, nonequilibrium situation. We consider interaction strengths of U/Γ up to 8 (we keep $U=4$ fixed and vary Γ). For these interaction strengths, we always find a stable nonmagnetic *GW* solution, i.e., $G_{\uparrow\uparrow} = G_{\downarrow\downarrow}$. In contrast, the HF solution can develop a magnetic moment for $U/\Gamma > \pi$ (depending on bias voltage and ε_c). We adopt the wide-band approximation where the coupling to the continuum is modeled by constant imaginary self-energies $\Sigma_L + \Sigma_R = -i\Gamma$. Without loss of generality, we set $E_F = 0$. In all calculations, the frequency grid extends from -15 to 15 with the grid spacing ranging from 0.1 to 0.0005.

A. Equilibrium spectral function

In Fig. 4, we show the ε_c dependence of the equilibrium spectral function, $A(\omega) = -\mathrm{Im}\, G^r(\omega)$, for $U=4$ and $\Gamma = 0.65$. The HF solutions are Lorentzians centered at $\varepsilon_{\mathrm{HF}} = \varepsilon_c + U\langle \hat{n}_\sigma \rangle$ with a full width at half maximum (FWHM) given by 2Γ. As can be seen, the position of the HF peaks do not vary linearly with ε_c. Instead, there is a "charging resistance" for the peak to move through the Fermi level due to the cost in Hartree energy associated with the filling of the level. This effectively pins the level to E_F.

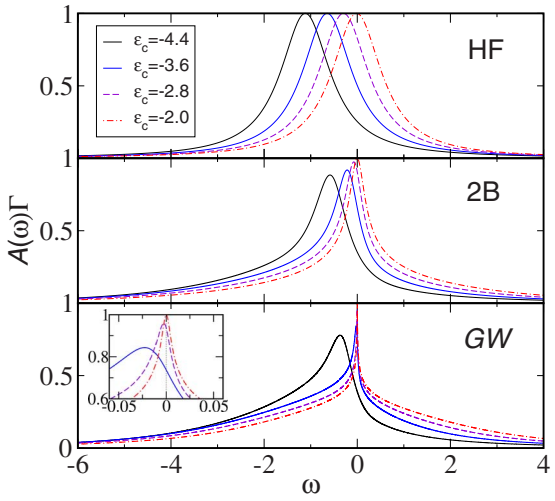

FIG. 4. (Color online) Spectral function of the central site for $\Gamma=0.65$, $U=4.0$, and different values of ε_c. The inset in the lower panel is a zoom of the *GW* spectral peak around $\omega=0$.

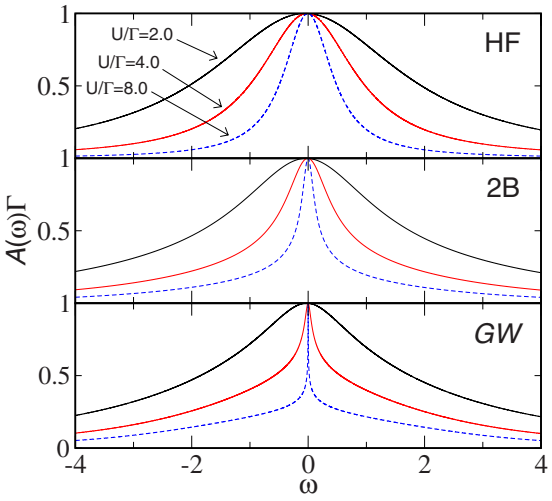

FIG. 6. (Color online) Spectral function for $U=4.0$, $\varepsilon_c=-U/2$, and three different values of $\Gamma=2.0$, 1.0, and 0.5 corresponding to strong, intermediate, and weak coupling to the leads.

Moving from HF to the second Born approximation, the Lorentzian shape of the spectral peak is distorted due to the ω dependence of the $2B$ self-energy. We can observe a general shift of spectral weight toward the chemical potential as well as a narrowing of the resonance as it comes closer to E_F.

The redistribution of the spectral weight toward the chemical potential becomes even more pronounced in the *GW* approximation. For $\Gamma-U<\varepsilon_c<-\Gamma$ (the so-called Kondo regime), a sharp peak develops at E_F. For U/Γ sufficiently large, the Kondo effect should reveal itself as a peak in the spectral function with a FWHM given approximately by the Kondo temperature[68]

$$T_K \approx 0.5(2\Gamma U)^{1/2} \exp[\pi\varepsilon_c(\varepsilon_c+U)/2\Gamma U]. \qquad (69)$$

In Fig. 5, we compare the above expression for T_K with the FWHM of the *GW* Kondo peak. The exponential scaling of T_K is surprisingly well reproduced. Deviations from the exponential scaling naturally occur for smaller values of U/Γ (not shown), where the Kondo effect does not occur and (69) does not apply. In accordance with recent work,[67] we were not able to obtain nonmagnetic *GW* solutions in the strong interaction regime ($U/\Gamma>8$).

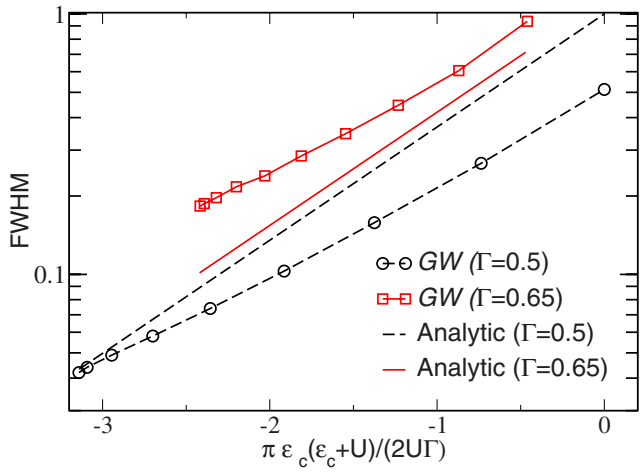

FIG. 5. (Color online) FWHM of the Kondo resonance as calculated in the *GW* approximation and from the analytical result Eq. (69). The interaction strength is $U=4$ and ε_c is varied in the Kondo regime.

In Fig. 6, we show the dependence of the spectral function on the ratio U/Γ for the central level at the symmetric position $\varepsilon_c=-U/2=-2$. For $U/\Gamma=2$, there is no significant difference between the three descriptions. This is to be expected since the correlation plays a minor role compared to the hybridization effects. In the weakly coupled limit, however, correlations become significant and, as a consequence, the $2B$ and *GW* results change markedly from the Lorentzian shape and show a Kondo-like peak at the metal Fermi level. The 2B approximation significantly overestimates the width of the Kondo peak, indicating, as expected, that the higher-order RPA terms enhance the strong correlation features.

For large U/Γ, it is known[36,57] that the spectral function, in addition to the Kondo peak, should develop peaks at the atomic levels ε_c and ε_c+U. We find that the self-consistent 2B and *GW* approximations always fail to capture these sidebands and instead distribute the spectral weight as a broad slowly decaying tail. These findings agree well with previous results obtained with the fluctuation-exchange approximation[69] and with *GW* studies of the homogeneous electron gas, which showed that self-consistency in the *GW* self-energy washed out the satellite structure in the spectrum.[70]

B. Nonequilibrium transport

We now move to the nonequilibrium case and introduce a difference in the chemical potentials of the two leads. In Fig. 7, we show the zero-temperature differential conductance under a symmetric bias, $\mu_{L/R}=\pm V/2$, as a function of ε_c for $U=4$ and $\Gamma=0.65$. The dI/dV at bias voltage V has been

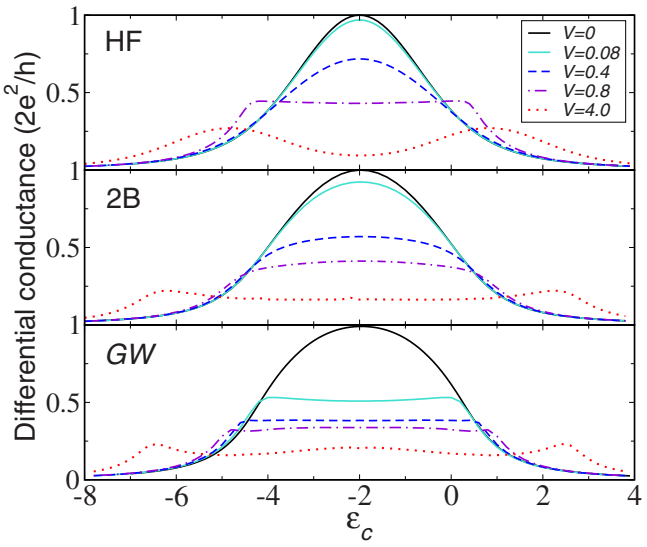

FIG. 7. (Color online) Differential conductance, dI/dV, as a function of the central site energy, ε_c, for different applied biases, $U=4$ and $\Gamma=0.65$.

calculated as a finite difference between the currents obtained from Eq. (51) for bias voltages V and $V+\delta V$, respectively. The 2B result falls in between the HF and GW results, and for this reason, we will focus on the latter two in the following discussion.

For $V=0$, there is only little difference between the three results, which all show a broad conductance peak reaching the unitary limit at the symmetric point $\varepsilon_c=-U/2$. The physical origin of the conductance trace is, however, very different: While the HF result is produced by coherent transport through a broad spectral peak moving rigidly through the Fermi level, the GW result is due to transport through a narrow Kondo peak which is always on resonance (for ε_c in the Kondo regime). In all cases, the width of the dI/dV curve is approximately U. In the GW case, this is because the Kondo peak develops only when the central level is half occupied, i.e., $-U\lesssim\varepsilon_c\lesssim 0$. In HF, on the other hand, the dI/dV peak acquires a width on the order of U due to the charge pinning effect discussed in Sec. VI A.

The difference in the mechanisms leading to the HF and GW results is brought out clearly as V is increased: for $V\ll\Gamma$, the bias has little effect on the HF conductance, while the GW conductance drops dramatically already at biases comparable to T_K due to the suppression of the Kondo resonance at finite bias. The suppression of the Kondo resonance is due to quasiparticle (QP) scattering. While QP scattering does not affect the lifetime of QPs at E_F in equilibrium, it does so at finite bias, where $\mathrm{Im}\,\Sigma_{GW}(E_F)$ becomes nonzero. We mention that we do not observe a splitting of the GW Kondo resonance at finite V.[62]

The peaks appearing in the dI/dV at the largest bias ($V=4$) occur when the central level is aligned with either the lower or upper edge of the bias window. It is worth noticing that the height of these peaks are smaller than the value of $1G_0$ expected from on-resonant transport through a single level. The reason for this is twofold: (i) The bias window only hits the resonance with one edge (either upper or lower edge), and consequently, only half the spectral weight enters the bias window when the voltage is increased by ΔV as compared to the low-bias situation. (ii) The self-consistent charging resistance discussed in Sec. VI A pins the level to the edge of the bias window, making the resonance follow the bias.

C. G_0W_0 approximation

Non-self-consistent, or one-shot, GW calculations can be performed by evaluating the screened interaction and GW self-energy from some trial noninteracting Green's function G_0. The resulting G_0W_0 approximation, with G_0 obtained from a local density approximation (LDA) and/or generalized gradient approximation (GGA) calculation, has been found to yield very satisfactory results for the band gaps of insulators and semiconductors.[31,32] For this reason, and due to its significantly lower computational cost, this G_0W_0 approach has generally been preferred over the self-consistent GW. One rather unsatisfactory feature of the perturbative G_0W_0 method is its G_0 dependence. However, as will be demonstrated below, a just as critical problem in nonequilibrium situations is its nonconserving nature.

Before we apply the G_0W_0 approximation to the Anderson model, we need to address a certain issue which unfortunately has led to an error in our previous paper.[27] (All conclusions from that paper are, however, unaffected by the mistake.)

1. Instability of the nonmagnetic ground state

Consider a system which admits a spin-polarized ground state at the Hartree level [notice that Hartree and HF is equivalent for the Anderson model when the effective interaction of Eq. (31) is used], and let G_0 denote the GF obtained from spin-unpolarized Hartree calculation. It turns out that the analytical properties of the screened interaction, $W_0^r[G_0]$, evaluated from G_0 will be wrong. In particular, $W_0^r[G_0]$ will not be retarded as it should be. The reason is that the RPA response function is ill defined around the nonmagnetic, and thus unstable, G_0. The problem has been previously mentioned by White[69] and was brought to the authors attention by Spataru.

For certain parameter values, the HF ground state of the Anderson model develops a finite magnetic moment. As a consequence, the analytic properties of W_0^r as calculated from Eq. (38) with the *unpolarized* G_{HF} become wrong. In our previous paper,[27] this problem was not recognized because we, for numerical efficiency, applied the Kramers–Kronig relation (47) to obtain Σ^r from $\Sigma^<-\Sigma^>$, instead of using Eq. (36). Thus, by construction, our Σ^r was retarded. Specifically, this implies that the G_0W_0 spectral function plotted in Fig. 1 of Ref. 27 as well as the dI/dV curves in the middle panel of Fig. 2 for ε_c in the interval -3.6 to -0.4 are incorrect. In fact, there exists no nonmagnetic $G_0W_0[G_{\mathrm{HF}}]$ solution in these cases. We stress, however, that all conclusions from our paper are unaffected by this mistake. In particular, we show below that for parameter values leading to a *stable* nonmagnetic HF ground state, the G_0W_0 approxima-

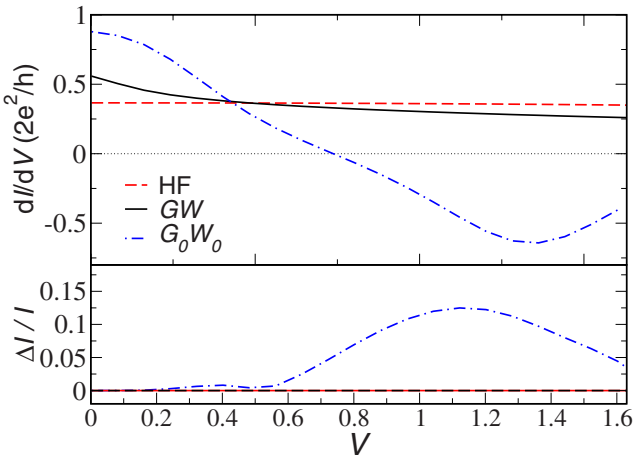

FIG. 8. (Color online) Differential conductance as a function of applied bias for $U=4$, $\Gamma=0.65$, and $\varepsilon_c=-4$. For these parameters, the nonmagnetic HF solution is stable for bias voltages smaller than ~ 1.6. The G_0W_0 approximation yields different currents at the left and right interfaces ($\Delta I \neq 0$) and yields negative differential conductance at finite bias.

tion still violates charge conservation and gives unphysical results such as negative differential conductance. Moreover, we arrive at the same conclusions for G_0W_0 self-energies constructed from the *spin-polarized* HF Green's function, in which case the instability problem does not occur at all.

2. Results of the G_0W_0 approximation

In Fig. 8, we show the calculated dI/dV for the Anderson model with $\Gamma=0.65$ and $\varepsilon_c=-4$ for the HF, *GW*, and $G_0W_0[G_{\mathrm{HF}}]$ approximations. For these parameters, the nonmagnetic HF solution is stable for bias voltages smaller than ~ 1.6 such that the G_0W_0 approximation based on a nonmagnetic G_{HF} is indeed meaningful in this parameter range. The G_0W_0 conductance has been obtained as a finite difference between the currents obtained from Green's functions with self-energies $\Sigma_{GW}[G_{\mathrm{HF}}(V)]$ and $\Sigma_{GW}[G_{\mathrm{HF}}(V+\delta V)]$, respectively, where $G_{\mathrm{HF}}(V)$ is the HF Green's function evaluated self-consistently under a bias voltage V.

From Fig. 8 we conclude that the G_0W_0 approximation leads to unphysical results in the form of strong negative differential conductance. Moreover, as shown in the lower panel of the figure, the G_0W_0 approach gives different values for I_L and I_R. We note in passing that this symmetry break comes from the different chemical potentials of the left and right leads. Finally, we mention that the increasing behavior of $\Delta I/I$ as a function of bias voltage seems to be a general effect.

As already mentioned, the HF solution breaks the spin symmetry for certain parameter values. Meaningful G_0W_0 results can still be obtained in this case provided the self-energy is constructed from the spin-polarized HF Green's function. Figures 9 and 10 compare the result of such calculations with self-consistent *GW* for two different values of the bias voltage. From the figures, we draw the following conclusions: (i) The G_0W_0 and *GW* currents agree when the level is almost empty or filled. (ii) The current calculated in

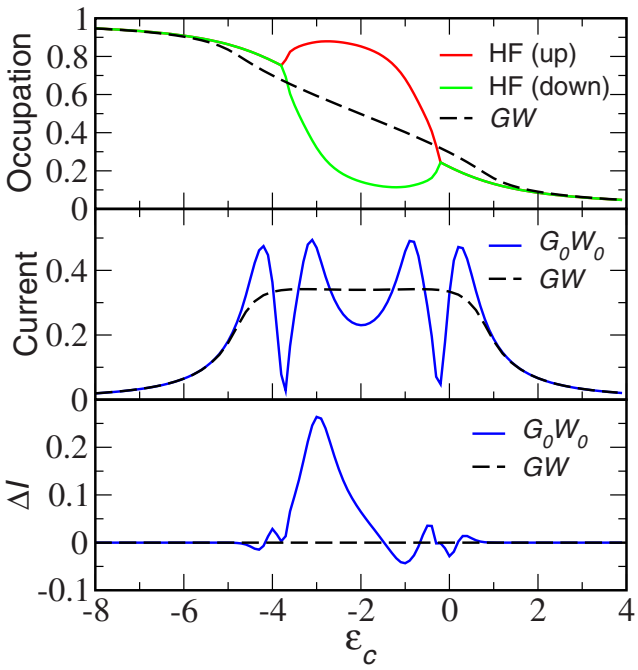

FIG. 9. (Color online) Upper panel: Occupation of the central site as function of ε_c for $U=4$, $\Gamma=0.65$, and bias $V=0.8$. Notice that the HF solution breaks the spin symmetry for some ε_c values. Middle panel: Current calculated in self-consistent *GW* and $G_0W_0[G_{\mathrm{HF},\uparrow}, G_{\mathrm{HF},\downarrow}]$. Lower panel: Violation of the continuity equation measured as the difference between the currents in the left and right leads.

G_0W_0 show unphysical behavior in and close to the magnetic regime. (iii) The violation of charge conservation in G_0W_0 is more severe when the current is large.

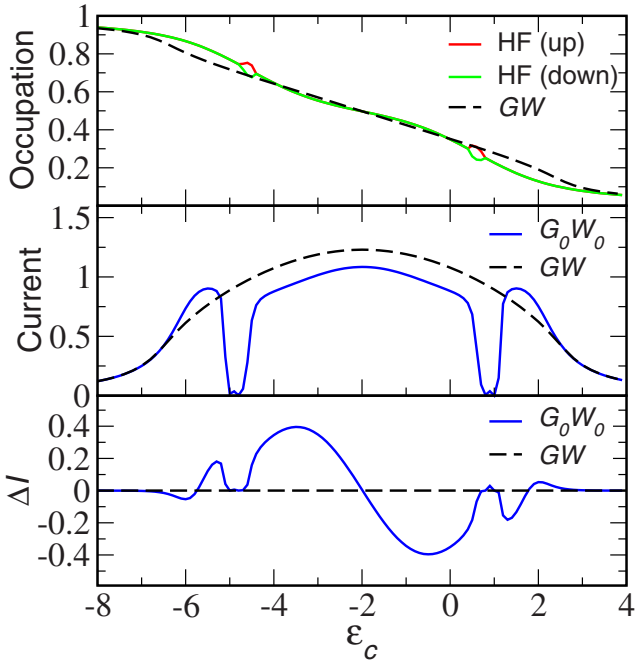

FIG. 10. (Color online) Same as Fig. 9, but for bias voltage $V=4.0$.

VII. BENZENE JUNCTION

In this section, we apply the Wannier-*GW* method to a more realistic nanojunction, namely, a benzene molecule coupled to featureless leads. In contrast to the Anderson model considered in the preceding section, the benzene junction represents a closed-shell system with the Fermi level lying within the HOMO-LUMO gap, leading to rather low transmission for all but the strongest molecule-lead coupling strengths.

The use of featureless (wide-band) electrodes is convenient as it allows us to isolate the effects of the electron-electron interactions. The use of more realistic contacts with energy dependent spectral features would lead to an additional renormalization of the molecular levels, making a clear separation between xc and contact effects more difficult. We stress, however, that the contacts only enter the theory through the coupling self-energies, which can be calculated once and for all as in the standard NEGF-DFT approach. Thus, the use of more realistic contact self-energies is straightforward.

To describe the benzene molecule, we first perform a DFT calculation for the isolated molecule (see Ref. 74). The KS eigenstates are then transformed into maximally localized WFs, and the KS Hamiltonian and Coulomb integrals are evaluated in the WF basis. For the interactions, we use the truncation scheme $\hat{V}^{(2)}$ defined in Appendix A to evaluate Hartree and exchange self-energies. As shown in Table I, this leads to results within ~5% of the exact values. We use the effective interaction Eq. (31) for the correlation part of the *GW* self-energy. In all calculations, we have applied a frequency grid extending from −100 to 100 eV and grid spacings in the range 0.2 to 0.02, depending on the value of Γ.

In Sec. VII A, we show that the experimental ionization potential of the isolated benzene molecule is very well reproduced with our *GW* scheme. In Sec. VII B, we investigate the role of the coupling strength Γ on the spectrum of the benzene junction. Finally, in Sec. VII C, we calculate the nonequilibrium conductance of the junction and we compare various approximations for the xc self-energy.

A. Spectrum of isolated benzene

Within our general transport formalism, we model the situation of a free molecule by using a very weak coupling to the wide-band leads [see Fig. 11(a)]. The contacts merely act as particle reservoirs fixing the number of electrons on the molecule and providing an insignificant broadening ($\Gamma = 0.05$ eV) of the discrete energy levels. We fix the Fermi levels of the electrodes to $E_F = -3$ eV, which is approximately halfway between the HOMO and LUMO levels (the precise position of E_F within the gap is unimportant for the results presented in this section).

In Fig. 12, we show the total density of states (DOS),

$$D(\varepsilon) = -\frac{1}{\pi}\sum_{n=1}^{N_w} \mathrm{Im}\, G^r_{nn}(\varepsilon), \tag{70}$$

where the sum runs over all WFs on the molecule. We use three different approximations: (i) DFT-PBE, (ii) Hartree–Fock, and (iii) fully self-consistent *GW*. We stress that our calculations include the full dynamical dependence of the *GW* self-energy as well as all off-diagonal elements. Thus, no analytic extension is performed, and we do not linearize the self-energy around the DFT eigenvalues to obtain an approximate quasiparticle equation as is done in standard *GW* calculations.

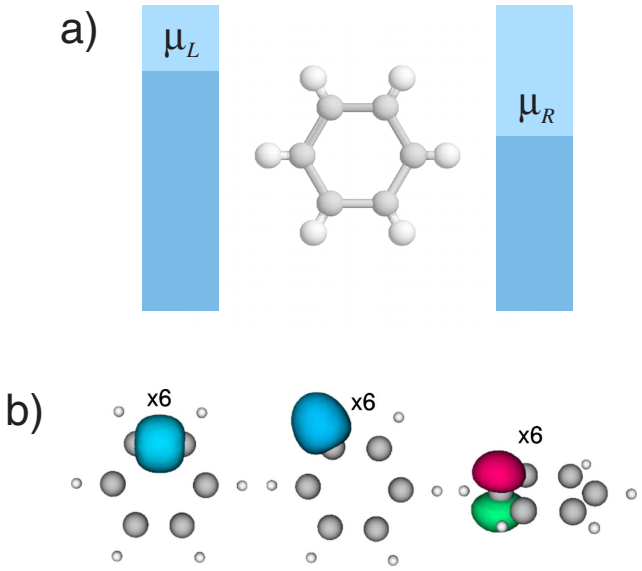

FIG. 11. (Color online) (a) Illustration of a benzene molecule coupled to featureless electrodes with different chemical potentials. (b) Isosurfaces for the 18 partially occupied Wannier functions used as basis functions in the calculations. The WFs are linear combinations of Kohn–Sham eigenstates obtained from a DFT-PBE plane-wave calculation.

The spectral peaks seen in Fig. 12 occurring above (below) the Fermi level correspond to electron addition (removal) energies. In particular, the HOMO level should coin-

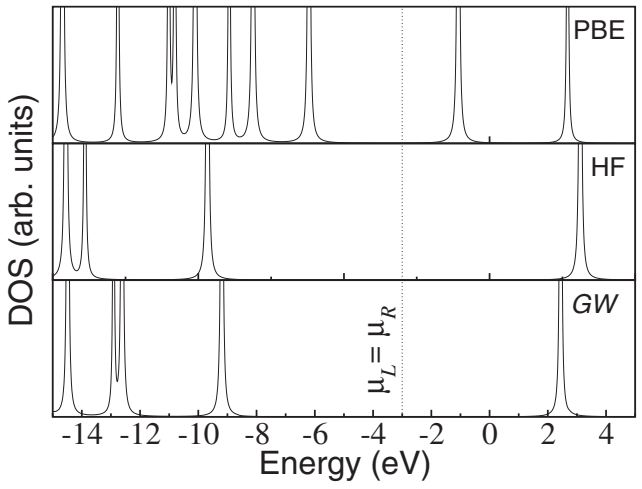

FIG. 12. Density of states for a benzene molecule weakly coupled to featureless leads (Γ=0.05). The common Fermi levels of the leads is indicated. Notice the characteristic opening of the band gap when going from DFT-PBE to HF and the subsequent (slight) reduction when correlations are included at the *GW* level.

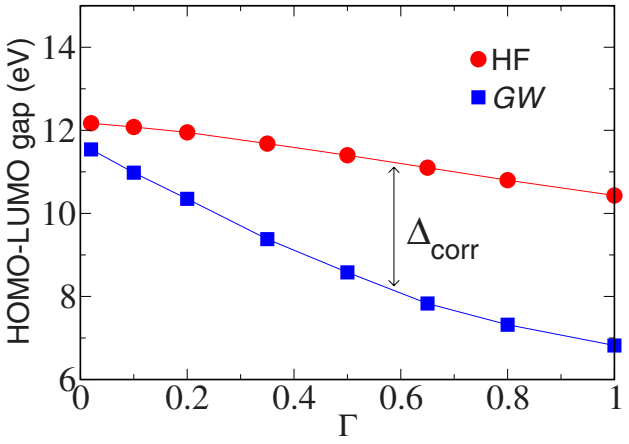

FIG. 13. (Color online) The HF and *GW* HOMO-LUMO gap of the benzene molecule as a function of the coupling strength Γ. The difference between the curves represents the reduction in the gap due to the correlation part of the *GW* self-energy. This value increases with the coupling strength as screening by electrons in the leads becomes more effective.

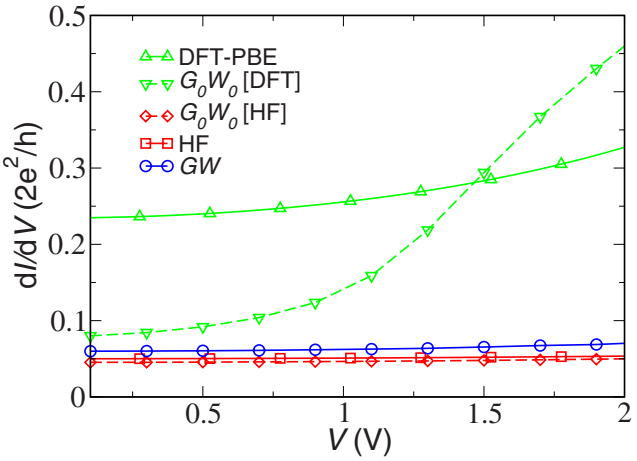

FIG. 14. (Color online) Differential conductance of the benzene junction for $\Gamma_L=\Gamma_R=0.25$ eV. Notice the strong G_0 dependence of the G_0W_0 result.

cide with the (vertical) ionization energy of the isolated molecule, which in the case of benzene is $I_{\mathrm{exp}}=-9.2$ eV.[71] The PBE functional overestimates this value by 3 eV, giving $I_{\mathrm{PBE}}=-6.2$ eV in good agreement with previous calculations.[30] The HF and *GW* calculation yields $I_{\mathrm{HF}}=-9.7$ eV and $I_{GW}=-9.3$ eV, respectively. Because of the limited size of the WF basis, the very good agreement between the *GW* and experimental values should not be taken too strict. Indeed, more accurate HF calculations predict a HOMO level around −9.2 eV, which is 0.5 eV higher than our HF result. The deviation of our HF calculation from this number is twofold: (i) The use of the truncated interaction $V^{(2)}$ to evaluate the exchange self-energy introduces an error of ~0.1 eV (see Table I). (ii) The difference between the PBE orbitals (from which our WFs are constructed) and the true HF orbitals.

Returning to Fig. 12, we notice a dramatic opening of the HOMO-LUMO gap when going from PBE to HF (and *GW*). This effect is due to the inability of the local xc-functionals to fully cancel the spurious self-interaction contained in the Hartree potential. For the same reason, the self-interaction-free HF method generally yields better spectra than the LDA and/or GGA functionals for small, localized systems where self-interaction terms are significant and dynamic screening is small. The *GW* spectrum resembles the HF spectrum with a slight reduction of the gap by ~1.0 eV. As we will show in the next section, the *GW* gap shrinks as the coupling strength Γ is increased.

B. Contact enhanced screening: The role of Γ

In Fig. 13, we plot the size of the HOMO-LUMO gap as a function of the coupling strength Γ. Both the HF and *GW* gaps decrease as Γ is increased. For the HF gap, this is a simple consequence of the redistribution of charge from the HOMO to the LUMO when the resonances broaden and their tails start to cross the Fermi level. As this happens, the HOMO (LUMO) self-interaction term in Σ_x will become less (more) negative and, consequently, the HF gap shrinks.

The *GW* quasiparticle energies consist of a HF eigenvalue and a correlation contribution coming from the real part of the dynamic *GW* self-energy,

$$\varepsilon^n_{\mathrm{QP}} = \varepsilon^n_{\mathrm{HF}} + \Delta^n_{\mathrm{corr}}. \tag{71}$$

According to Fig. 13, the correlation part of the QP gap,

$$\Delta_{\mathrm{corr}} = \Delta^{\mathrm{HOMO}}_{\mathrm{corr}} - \Delta^{\mathrm{LUMO}}_{\mathrm{corr}}, \tag{72}$$

increases significantly with Γ. In fact, for a large range of coupling strengths, the reduction of the gap is more than 3 eV. This reduction can be understood from the enhanced mobility of the electrons on the molecule when the coupling is strong. The enhanced mobility allows for more efficient screening and this reduces the QP gap. The difference between the large- and small-Γ limits is analogous to the difference between extended and confined systems. In extended systems where screening is significant, band gaps are overestimated by HF and correlation contributions to the gap are large. In confined systems, such as atoms and small molecules, screening effects are unimportant and HF usually yields good HOMO-LUMO gaps.

C. Conductance

In this section, we consider the transport properties of the benzene junction under a symmetric bias, $\mu_{L/R}=\pm V/2$, and a coupling strength of $\Gamma_L=\Gamma_R=0.25$ eV.

In Fig. 14, we compare the differential conductance, dI/dV, calculated in self-consistent DFT-PBE, HF, and *GW* as well as non-self-consistent G_0W_0 using either the DFT-PBE or HF Green's function as G_0. The dI/dV has been obtained by numerical differentiation of the $I(V)$ curves calculated from Eq. (51). For the DFT calculation, the finite-bias effects have been included at the Hartree level, i.e., changes in the xc potential have been neglected. We notice

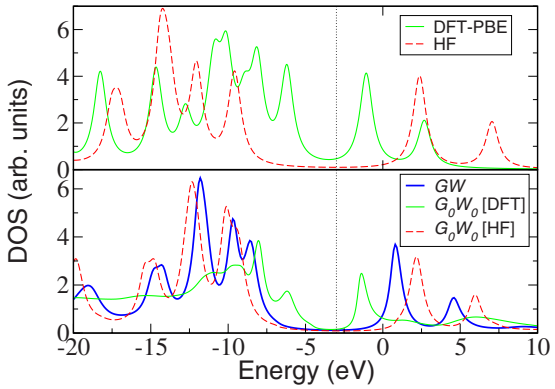

FIG. 15. (Color online) Equilibrium DOS for the benzene molecule coupled to wide-band leads with a coupling strength of $\Gamma_L = \Gamma_R = 0.25$ eV. Upper panel shows DFT-PBE and HF single-particle approximations, while the lower panel shows the self-consistent *GW* result as well as the one-shot G_0W_0 results based on the DFT and HF Green's functions, respectively.

that the HF and $G_0W_0[G_{\mathrm{HF}}]$ results are close to the self-consistent *GW* result. These approximations all yield a nearly linear *I-V* with a conductance of $\sim 0.05G_0$. In contrast, the DFT and $G_0W_0[G_{\mathrm{DFT}}]$ yield significantly larger conductances which increase with the bias voltage. We note that the violation of charge conservation in the G_0W_0 calculations is not too large in the present case ($\Delta I/I < 5\%$). This is in line with our general observation, e.g., from the Anderson model, that $\Delta I/I$ grows with I.

The trends in conductance can be understood by considering the (equilibrium) DOS of the junction shown in Fig. 15. As for the free benzene molecule (see Fig. 12), the DFT HOMO-LUMO gap is much smaller than the HF gap, and this explains the lower conductance found in the latter case. The *GW* gap falls in between the DFT and HF gaps; however, the magnitude of the DOS at E_F is very similar in *GW* and HF, which is the reason for the similar conductances. It is interesting to notice that the HOMO-LUMO gap obtained in the G_0W_0 calculations resemble the gap obtained from G_0 and that the self-consistent *GW* gap lies in between the $G_0W_0[G_{\mathrm{DFT}}]$ and $G_0W_0[G_{\mathrm{HF}}]$ gaps.

The increase in the $G_0W_0[G_{\mathrm{DFT}}]$ conductance as a function of bias occurs because the LUMO of the $G_0W_0[G_{\mathrm{DFT}}]$ calculation moves downward into the bias window and becomes partly filled as the voltage is raised. In a self-consistent calculation, this would lead to an increase in Hartree potential which would, in turn, raise the energy of the level. The latter effect is missing in the perturbative G_0W_0 approach, and this can lead to uncontrolled changes in the occupations as the present example shows.

Finally, we notice that the $G_0W_0[G_{\mathrm{DFT}}]$ DOS is significantly more broadened than both the $G_0W_0[G_{\mathrm{HF}}]$ and *GW* DOSs. The reason for this is that the DFT DOS has a relatively large weight close to E_F. This enhances the QP scattering and leads to shorter lifetimes of the QP in the $G_0W_0[G_{\mathrm{DFT}}]$ calculation. Noticing that the QP lifetime is inversely proportional to $\mathrm{Im}\,\Sigma_{GW}$ explains the broadening of the spectrum.

VIII. CONCLUSIONS

With the aim of investigating the role of electronic correlations in quantum transport, we have implemented the nonequilibrium *GW* approximation to the electronic self-energy of a finite region of interacting electrons coupled to noninteracting leads. We have shown, both analytically and numerically, that the self-consistent *GW* self-energy leads to identical currents at the left and right interfaces of the central region. In contrast, the widely used G_0W_0 self-energy does not conserve the particle number and, thus, violates the continuity equation. More generally, we have shown that any Φ-derivable self-energy will yield identical left and right currents independent of the basis set applied.

Using a WF basis, we have introduced an effective electron-electron interaction which resembles the real-space representation, but is spin dependent and self-interaction-free in the WF basis. In general, this provides a means for reducing self-interaction errors in diagrammatic approaches such as the *GW* method.

The *GW* method was applied to the Anderson impurity model. In equilibrium and $T=0$, we found that the self-consistent *GW* approximation describes the width of the Kondo resonance well for intermediate interaction strengths, $U=4$ and $\Gamma \gtrsim 0.5$. On the other hand, the sidebands of the spectral function are always missing in *GW*. We presented nonequilibrium *I-V* curves, and we discussed the important effect of quasiparticle scattering under a finite bias which reduces the QP lifetimes, leading to a broadening of spectral features and a significant suppression of the finite-bias conductance. Finally, we demonstrated that the G_0W_0 approach can produce severe errors including violation of charge conservation and negative differential conductance. The errors become more significant at higher bias and close to magnetic transition points.

We investigated the properties of a molecular junction consisting of a benzene molecule sandwiched between featureless leads. To describe the benzene, we used a minimal Wannier function basis set which was shown to reproduce the exact Hartree and exchange matrix elements to within 5%. The calculated ionization potential in *GW* was found to be in good agreement with the experimental value. A significant reduction of the *GW* HOMO-LUMO gap was observed for increasing molecule-lead coupling. The effect comes from the correlation part of the *GW* self-energy and reflects the more efficient screening in a strongly, compared to a weakly, coupled junction.

Finally, the nonequilibrium differential conductance of the benzene junction was calculated in DFT-PBE, HF, and *GW* as well as in G_0W_0[HF] and G_0W_0[DFT]. It was found that HF and G_0W_0[HF] yield results similar to *GW*, while both DFT and G_0W_0[DFT] yield significantly larger conductances. In particular, this shows that the G_0 dependence of the G_0W_0 approximation should not be disregarded. The trends in conductance were explained in terms of the size of the HOMO-LUMO gap of the molecule, which also shows significant variation depending on the approximation used.

ACKNOWLEDGMENTS

The authors thank E. K. U Gross, S. Kurth, G. Stefanucci,

TABLE I. Hartree and exchange energies in eV for five frontier molecular orbitals of the benzene molecule. The values are obtained using the truncated interactions defined in Eqs. (A1)–(A3) as well as the full interaction $\hat{V}$ (the exact result). For reference, the first column shows the eigenvalues as calculated using the PBE xc functional.

		$\langle\psi_n\|\Sigma_h\|\psi_n\rangle$				$\langle\psi_n\|\Sigma_x\|\psi_n\rangle$			
State (symmetry)	$\varepsilon_{\mathrm{DFT}}$	$\hat{V}^{(1)}$	$\hat{V}^{(2)}$	$\hat{V}^{(3)}$	Exact	$\hat{V}^{(1)}$	$\hat{V}^{(2)}$	$\hat{V}^{(3)}$	Exact
HOMO-2 (π)	−8.94	217.6	221.2	233.2	233.0	−14.6	−16.4	−16.3	−16.7
HOMO-1 (σ)	−8.12	253.6	244.7	224.7	224.6	−24.7	−20.2	−20.2	−19.6
HOMO (π)	−6.20	220.1	223.0	229.5	229.5	−13.7	−15.2	−15.0	−15.1
LUMO (π^*)	−1.08	222.1	222.7	219.1	219.3	−7.2	−7.5	−7.5	−7.2
LUMO+1 (π^*)	2.68	223.1	221.4	199.3	199.7	−6.1	−5.3	−5.8	−4.7
Average deviation (%)		7.3	5.8	0.1		15.5	4.5	6.7	

R. Godby, A. Feretti, A.-P. Jauho, and K. Kaasbjerg for useful discussions. We thank Catalin Spataru for pointing out the problem related to the instability of nonmagnetic HF ground state, and Carsten Rostgaard for discussions concerning the evaluation of Coulomb integrals. K.S.T. acknowledges support from the Danish Natural Science Research Council and from the Danish Center for Scientific Computing through Grant No. HDW-1103-06. The Center for Atomic-scale Materials Design (CAMD) is sponsored by the Lundbeck Foundation. A.R. acknowledges support from the EC Network of Excellence NANOQUANTA (Ref. No. NMP4-CT-2004-500198), the Spanish Ministry of Education (Grant No. FIS2007-65702-C02-01), the SANES (Ref. No. NMP4-CT-2006-017310), the DNA-NANODEVICES (Ref. No. IST-2006-029192), the NANO-ERA Chemistry projects, the University of the Basque Country EHU/UPV (SGIker Arina), and the Basque Country Government, and the computer resources, technical expertise, and assistance provided by the Barcelona Supercomputing Center-Centro Nacional de Supercomputación.

APPENDIX A: HARTREE AND EXCHANGE POTENTIALS

In this work, the exchange and Hartree self-energies have been evaluated from Eqs. (45) and (46) with the Coulomb matrix elements restricted to a certain subset (the set $\hat{V}^{(2)}$ defined below). Here, we investigate the quality of such approximations by testing their ability to reproduce Hartree and exchange energies of the molecular orbitals of a benzene molecule.[74] We, thus, consider the following truncation schemes:

$$\hat{V}^{(1)} = \hat{V}[\{V_{ij,ij}\},\{V_{ij,ji}\}], \tag{A1}$$

$$\hat{V}^{(2)} = \hat{V}[\{V_{ij,ij}\},\{V_{ij,ji}\},\{V_{ii,jj}\},\{V_{ii,ij}\}], \tag{A2}$$

$$\hat{V}^{(3)} = \hat{V}[\{V_{ij,ij}\},\{V_{ij,ji}\},\{V_{ii,jj}\},\{V_{ii,ij}\},\{V_{ik,jk}\}], \tag{A3}$$

where, e.g., the notation $\hat{V}[\{V_{ij,ij}\}]$ means that all elements of the form $V_{ij,ij}$ are included in the sum in Eq. (3).

The molecular orbitals of benzene, $\{\psi_n\}$, can, by construction of the WFs $\{\phi_i\}$, be exactly expanded as

$$\psi_n(\mathbf{r}) = \sum_i c_{in}\phi_i(\mathbf{r}). \tag{A4}$$

The 18 WFs used to describe the benzene molecule are plotted in Fig. 11(b). For the molecular orbital ψ_n, we can then calculate the exact Hartree and exchange energies from

$$\langle\psi_n|\Sigma_h|\psi_n\rangle = 2\sum_m^{\mathrm{occ}} \int d\mathbf{r}d\mathbf{r}' \frac{\psi_n(\mathbf{r})^*\psi_m(\mathbf{r}')^*\psi_m(\mathbf{r}')\psi_n(\mathbf{r})}{|\mathbf{r}-\mathbf{r}'|},$$

$$\langle\psi_n|\Sigma_x|\psi_n\rangle = -\sum_m^{\mathrm{occ}} \int d\mathbf{r}d\mathbf{r}' \frac{\psi_n(\mathbf{r})^*\psi_m(\mathbf{r}')^*\psi_m(\mathbf{r})\psi_n(\mathbf{r}')}{|\mathbf{r}-\mathbf{r}'|}.$$

Alternatively, we can insert the expansion (A4) and get

$$\langle\psi_n|\Sigma_h|\psi_n\rangle = \sum_{ij} c_{in}^*\Sigma_{h,ij}c_{jn}, \tag{A5}$$

$$\langle\psi_n|\Sigma_x|\psi_n\rangle = \sum_{ij} c_{in}^*\Sigma_{x,ij}c_{jn}, \tag{A6}$$

where $\Sigma_{h,ij}$ and $\Sigma_{x,ij}$ are the self-energies in the WF basis obtained from Eqs. (45) and (46). The latter are approximated by the truncation schemes (A1)–(A3) for the Coulomb integrals, $V_{ij,kl}$.

In Table I, we compare the exact values of the Hartree and exchange matrix elements for the frontier molecular orbitals to the approximate ones, obtained using the truncated interactions. We note that $\hat{V}^{(2)}$, which is the truncation scheme we have used, leads to average deviations around 5%.

As a final remark, we notice that our results for $\langle\psi_n|\Sigma_x|\psi_n\rangle$ evaluated using $\hat{V}^{(1)}$ provides roughly the same accuracy as a recently developed method combining tight-binding DFT with *GW*.[30]

APPENDIX B: ASSESSMENT OF EFFECTIVE INTERACTION

As discussed in Sec. III A, the *GW* approximation includes only a single diagram at each order of the interaction. The error resulting from such an approximation is—to lowest order—similar to the error of approximating a HF calcu-

TABLE II. Left part: Hartree self-energy for some of the frontier orbitals of the benzene molecule. The Hartree self-energy has been evaluated using the effective interaction Eq. (30), the effective interaction without the spin-dependent correction [second term in Eq. (31)], and using the full interaction Eq. (3) (exact result). Right: The exact value of the Hartree–Fock self-energy. Note that the spin-dependent correction term in $\hat{V}_{\text{eff}}$ cancels the self-interaction (in the local Wannier basis) and, thus, incorporates part of the exchange in the Hartree potential. Last row shows the average deviation of the Hartree potential from the exact Hartree–Fock potential.

	$\langle\psi_n\vert\Sigma_h\vert\psi_n\rangle$			$\langle\psi_n\vert\Sigma_h+\Sigma_x\vert\psi_n\rangle$
State (symmetry)	$\{V_{ij,ij}\}$	$\hat{V}_{\text{eff}}$	Exact	Exact
HOMO-2 (π)	217.6	207.4	233.0	216.3
HOMO-1 (σ)	253.9	230.1	224.6	205.0
HOMO (π)	220.7	210.1	229.5	214.4
LUMO (π^*)	222.8	212.2	219.3	212.1
LUMO+1 (π^*)	223.7	213.1	199.7	195.0
Average deviation (%) from exact HF (right column)	9.5	5.5	6.0	

lation by a Hartree calculation. It is not obvious that the best result of such an approximation is obtained by using the full interaction of Eq. (3). For example, such a strategy would lead to self-interaction errors.

In Table II (middle panel), we compare the Hartree matrix elements of some molecular orbitals of benzene,[74] evaluated using different effective interactions. Notice that the values listed in the two leftmost columns differ by the inclusion of the spin-dependent term of Eq. (31). In the right column, we show the exact HF result, i.e., the correct result to first order in the interaction. The last row shows the average deviation of the Hartree energies from the exact HF energies.

From Table II, we conclude that the effective interaction produces results of comparable accuracy to the full interaction if one attempts to reproduce the exact result to first order from the Hartree approximation only. The fact that $\hat{V}_{\text{eff}}$ performs better than $\{V_{ij,ij}\}$ indicates that the spin-dependent term in $\hat{V}_{\text{eff}}$, which removes the self-interaction in the WF basis, is significant.

Extrapolating these observations to higher order, we conclude that the use of $\hat{V}_{\text{eff}}$ in GW calculations should produce results comparable to GW calculations based on the full interaction.

At this point, we stress again that for practical calculations, we use the truncation scheme of Eq. (A2) for evaluating Hartree and exchange. Thus, the results presented in this section only serve to estimate the performance of the effective interaction for the higher-order GW diagrams.

APPENDIX C: A USEFUL RELATION

Let $B(\tau,\tau')$ and $C(\tau,\tau')$ be two matrix valued functions on the Keldysh contour and consider the commutator A defined by

$$A(\tau,\tau') = \int_{\mathcal{C}} [B(\tau,\tau_1)C(\tau_1,\tau') - C(\tau,\tau_1)B(\tau_1,\tau')]d\tau_1, \tag{C1}$$

where matrix multiplication is implied. Under steady state conditions where the real-time components of B and C can be assumed to depend only on the time difference $t'-t$, the following identity holds:

$$\mathrm{Tr}[A^<(t,t)] = \int \frac{d\omega}{2\pi}\mathrm{Tr}[B^<(\omega)C^>(\omega) - B^>(\omega)C^<(\omega)]. \tag{C2}$$

To prove this relation, we first use the Langreth rules to obtain

$$A^<(t,t') = \int [B^<(t,t_1)C^a(t_1,t') + B^r(t,t_1)C^<(t_1,t') - C^<(t,t_1)B^a(t_1,t') - C^r(t,t_1)B^<(t_1,t')]dt_1.$$

Since all quantities on the right hand side depend only on the time difference, we identify the integrals as convolutions which, in turn, become products when Fourier transformed. We, thus, have

$$\begin{aligned} A^<(t,t) &= \int \frac{d\omega}{2\pi}A^<(\omega) \\ &= \int \frac{d\omega}{2\pi}[B^<(\omega)C^a(\omega) + B^r(\omega)C^<(\omega) \\ &\quad - C^<(\omega)B^a(\omega) - C^r(\omega)B^<(\omega)]. \end{aligned}$$

Equation (C2) now follows from the cyclic property of the trace and the identity $G^r-G^a=G^>-G^<$.

APPENDIX D: COUPLING TO QUASIPERIODIC LEADS

We consider the coupling of the central region (C) to the left lead (L) in the case where L is periodic only beyond a certain transition region (T). We refer to the periodic parts of the lead as principal layers and denote the corresponding blocks of the Hamiltonian matrix by h_0. Without loss of generality, we assume nearest neighbor coupling between the principal layers and denote the coupling matrices by v_0. The transition region is assumed so large that there is no coupling across it, i.e., between the central region and the first principal layer. If this is not the case, the transition region must be extended by the first principal layer. The Hamiltonian of the left lead and its periodic part can then be written as

$$h_L = \begin{pmatrix} \ddots & \vdots & \vdots & \vdots \\ \cdots & h_0 & v_0 & 0 \\ \cdots & v_0^\dagger & h_0 & v_T \\ \cdots & 0 & v_T^\dagger & h_T \end{pmatrix}, \quad h_L^{per} = \begin{pmatrix} \ddots & \vdots & \vdots & \vdots \\ \cdots & h_0 & v_0 & 0 \\ \cdots & v_0^\dagger & h_0 & v_0 \\ \cdots & 0 & v_0^\dagger & h_0 \end{pmatrix}. \tag{D1}$$

The (retarded) GFs defined from h_L and h_L^{per} are denoted by $g_{0,L}$ and $g_{0,L}^{per}$, respectively. The lower right block of $g_{0,L}$,

corresponding to the transition region, is denoted by $[g_{0,L}]_T$ and the lower right block of $g^{per}_{0,L}$, corresponding to the first principal layer, is denoted by $[g^{per}_{0,L}]_0$. We have the following equation:

$$[g_{0,L}]_T = [(\omega + i\eta)I - h_T - \Sigma_T]^{-1}, \tag{D2}$$

where the self-energy is given by

$$\Sigma_T = v_T^\dagger [g^{per}_{0,L}]_0 v_T. \tag{D3}$$

In the above equation, $[g^{per}_{0,L}]_0$ can be obtained using the standard decimation technique.[72] The coupling self-energy Σ_L can now be constructed from $[g_{0,L}]_T$ and the matrices h_{TC} and h_{CT} which describe the coupling between the transition region in the left lead and the central region,

$$\Sigma^r_L = h_{CT}[g^r_{0,L}]_T h_{TC}. \tag{D4}$$

We remark that h_{CT} and h_{TC} are submatrices of h_{CL} and h_{LC}. Completely analog results hold for the coupling to the right lead (Fig. 16).

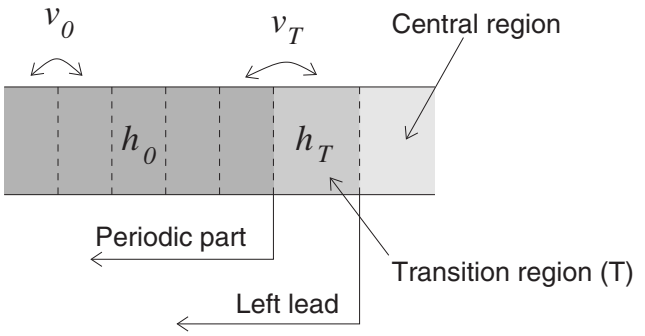

FIG. 16. The transition region, T, is defined as the part of the lead beyond which the lead Hamiltonian becomes periodic.

APPENDIX E: RETARDED FUNCTIONS FROM CORRELATION FUNCTIONS

In steady state, all four real-time GFs Eqs. (16)–(19) follow from the retarded and lesser components and, thus, it suffices to calculate these.

Given $G^r(\omega)$ and $G^<(\omega)$ sampled on an equidistant frequency grid, the corresponding *GW* self-energy, $\Sigma_{GW}[G](\omega)$, can be obtained from Eqs. (36)–(41) using the FFT to switch between energy and time domains. However, as an alternative to Eqs. (36) and (40), we have found it more useful to obtain Σ^r_{GW} and P^r from the relation

$$X^r(t) = \theta(-t)[X^>(t) - X^<(t)], \tag{E1}$$

which is valid for any function X on the Keldysh contour that does not contain delta functions. Note that when applied to Σ_{GW}, Eq. (E1) yields only the correlation part of Σ^r_{GW} as explained in Sec. III B. The reason why we prefer Eq. (E1) over equations (36) and (40) is that $X^r(\omega)$ falls off as $1/\omega$ (due to the step function in time), which makes it difficult to obtain a faithful representation of $X^r(t)$ from a FFT of $X^r(\omega)$. In contrast, $X^{</>}(\omega)$ are well localized (they are smooth in time) and the FFT can be safely used to obtain $X^{</>}(\omega)$ from $X^{</>}(t)$ and vice versa. It is possible to reduce the size of the frequency grid significantly if a zero padding of $X^{</>}(\omega)$ is introduced before the FFT is applied to obtain $X^{</>}(t)$.[73] As discussed in Sec. III B, Eq. (E1) with $X=\Sigma$ yields the correlation part of the *GW* self-energy. The static Hartree and exchange terms, Σ_h and Σ_x, are calculated from Eqs. (45) and (46). Once the self-energies have been calculated, a new set of GFs can be calculated from Eqs. (64) and (26).

[1] N. Agrait, A. L. Yeyati, and J. M. van Ruitenbeek, Phys. Rep. **377**, 81 (2003), and references therein.
[2] M. A. Reed, C. Zhou, C. J. Muller, T. P. Burgin, and J. M. Tour, Science **278**, 252 (1997).
[3] R. H. M. Smit, Y. Noat, C. Untiedt, N. D. Lang, M. C. van Hemert, and J. M. van Ruitenbeek, Nature (London) **419**, 906 (2002).
[4] J. Taylor, H. Guo, and J. Wang, Phys. Rev. B **63**, 245407 (2001).
[5] Y. Xue, S. Datta, and M. A. Ratner, Chem. Phys. **281**, 151 (2001).
[6] M. Brandbyge, J. L. Mozos, P. Ordejón, J. Taylor, and K. Stokbro, Phys. Rev. B **65**, 165401 (2002).
[7] K. S. Thygesen, M. V. Bollinger, and K. W. Jacobsen, Phys. Rev. B **67**, 115404 (2003).
[8] S. K. Nielsen, Y. Noat, M. Brandbyge, R. H. M. Smit, K. Hansen, L. Y. Chen, A. I. Yanson, F. Besenbacher, and J. M. van Ruitenbeek, Phys. Rev. B **67**, 245411 (2003).
[9] D. Djukic, K. S. Thygesen, C. Untiedt, R. H. M. Smit, K. W. Jacobsen, and J. M. van Ruitenbeek, Phys. Rev. B **71**, 161402(R) (2005); K. S. Thygesen and K. W. Jacobsen, Phys. Rev. Lett. **94**, 036807 (2005).
[10] M. Strange, K. S. Thygesen, and K. W. Jacobsen, Phys. Rev. B **73**, 125424 (2006).
[11] K. Stokbro, J. Taylor, M. Brandbyge, J.-L. Mozos, and P. Ordejón, Comput. Mater. Sci. **27**, 151 (2003).
[12] J. Heurich, J. C. Cuevas, W. Wenzel, and G. Schon, Phys. Rev. Lett. **88**, 256803 (2002).
[13] S. Y. Quek, L. Venkataraman, H. J. Choi, S. G. Louie, M. S. Hybertsen, and J. B. Neaton, Nano Lett. **7**, 3477 (2007).
[14] M. Koentopp, K. Burke, and F. Evers, Phys. Rev. B **73**, 121403(R) (2006).
[15] K. Hirose and M. Tsukada, Phys. Rev. Lett. **73**, 150 (1994).
[16] N. D. Lang, Phys. Rev. B **52**, 5335 (1995).
[17] H. J. Choi and J. Ihm, Phys. Rev. B **59**, 2267 (1999).
[18] R. Gebauer and R. Car, Phys. Rev. Lett. **93**, 160404 (2004).
[19] P. Delaney and J. C. Greer, Phys. Rev. Lett. **93**, 036805 (2004).
[20] M. H. Hettler, W. Wenzel, M. R. Wegewijs, and H. Schoeller, Phys. Rev. Lett. **90**, 076805 (2003).
[21] P. Bokes, J. Jung, and R. W. Godby, Phys. Rev. B **76**, 125433 (2007).
[22] F. Malet, M. Pi, M. Barranco, and E. Lipparini, Phys. Rev. B **72**, 205326 (2005).

[23] G. Stefanucci and C.-O. Almbladh, Phys. Rev. B **69**, 195318 (2004).
[24] M. Di Ventra and T. N. Todorov, J. Phys.: Condens. Matter **16**, 8025 (2004).
[25] S. Kurth, G. Stefanucci, C.-O. Almbladh, A. Rubio, and E. K. U. Gross, Phys. Rev. B **72**, 035308 (2005).
[26] P. Darancet, A. Ferretti, D. Mayou, and V. Olevano, Phys. Rev. B **75**, 075102 (2007).
[27] K. S. Thygesen and A. Rubio, J. Chem. Phys. **126**, 091101 (2007).
[28] G. Baym, Phys. Rev. **127**, 1391 (1962).
[29] J. B. Neaton, M. S. Hybertsen, and S. G. Louie, Phys. Rev. Lett. **97**, 216405 (2006).
[30] T. A. Niehaus, M. Rohlfing, F. Della Sala, A. Di Carlo, and Th. Frauenheim, Phys. Rev. A **71**, 022508 (2005).
[31] M. S. Hybertsen and S. G. Louie, Phys. Rev. B **34**, 5390 (1986).
[32] G. Onida, L. Reining, and A. Rubio, Rev. Mod. Phys. **74**, 601 (2002).
[33] A. Stan, N. E. Dahlen, and R. van Leeuwen, Europhys. Lett. **76**, 298 (2006).
[34] S. Kubatkin, A. Danilov, M. Hjort, J. Cornil, J.-L. Bredas, N. Stuhr-Hansen, P. Hedeård, and T. Bjørnholm, Nature (London) **425**, 698 (2003).
[35] D. Goldhaber-Gordon, Hadas Shtrikman, D. Mahalu, David Abusch-Magder, U. Meirav, and M. A. Kastner, Nature (London) **391**, 156 (1998).
[36] T. A. Costi, A. C. Hewson, and V. Zlatic, J. Phys.: Condens. Matter **6**, 2519 (1994).
[37] K. S. Thygesen, Phys. Rev. B **73**, 035309 (2006).
[38] R. van Leeuwen, N. E. Dahlen, G. Stefanucci, C. O. Almbladh, and U. von Barth, *Time-Dependent Density Functional Theory* (Springer, New York, 2006).
[39] H. Haug and A.-P. Jauho, *Quantum Kinetics in Transport and Optics of Semiconductors* (Springer, New York, 1998).
[40] A. L. Fetter and J. D. Walecka, *Quantum Theory of Many-Particle Systems* (McGraw-Hill, New York, 1971).
[41] G. Stefanucci, Phys. Rev. B **75**, 195115 (2007).
[42] W. Nelson, P. Bokes, Patrick Rinke, and R. W. Godby, Phys. Rev. A **75**, 032505 (2007).
[43] C. D. Spataru, L. X. Benedict, and S. G. Louie, Phys. Rev. B **69**, 205204 (2004).
[44] N. E. Dahlen and R. van Leeuwen, Phys. Rev. Lett. **98**, 153004 (2007).
[45] Y. Meir and N. S. Wingreen, Phys. Rev. Lett. **68**, 2512 (1992).
[46] We use $(G^a)^{-1}-(G^r)^{-1}=\Sigma^r_{tot}-\Sigma^a_{tot}=\Sigma^>_{tot}-\Sigma^<_{tot}$.
[47] K. S. Thygesen, L. B. Hansen, and K. W. Jacobsen, Phys. Rev. B **72**, 125119 (2005).
[48] B. Hammer, L. B. Hansen, and J. K. Nørskov, Phys. Rev. B **59**, 7413 (1999); S. R. Bahn and K. W. Jacobsen, Comput. Sci. Eng. **4**, 56 (2002). The DACAPO code can be downloaded at http://www.fysik.dtu.dk/campos.
[49] K. S. Thygesen and K. W. Jacobsen, Chem. Phys. **319**, 111 (2005).
[50] These six-dimensional integrals are evaluated in a two-step procedure: First, a Poisson equation for the (complex) charge distribution $\varrho_{ik}(\mathbf{r})=\phi_i(\mathbf{r})^*\phi_k(\mathbf{r})$ is solved to obtain the potential $v_{ik}(\mathbf{r})$. If the Poisson equation is solved in Fourier space, one must solve for the potential $\tilde{v}_{ik}$ of the neutralized charge $\tilde{\varrho}_{ik}=\varrho_{ik}-\varrho_{G,ik}$, where $\varrho_{G,ik}$ is a neutralizing Gaussian charge distibution for which the associated potential $v_{G,ik}$ is known analytically. In the last step, we obtain the Coulomb integral as $V_{ij,kl}=\int d\mathbf{r}\,\phi_j(\mathbf{r})^* v_{ik}(\mathbf{r})\phi_l(\mathbf{r})$.
[51] P. Pulay, Chem. Phys. Lett. **73**, 393 (1980).
[52] P. W. Anderson, Phys. Rev. **124**, 41 (1961).
[53] N. Andrei, K. Furuya, and J. H. Lowenstein, Rev. Mod. Phys. **55**, 331 (1983).
[54] A. M. Tsvelick and P. B. Wiegmann, Adv. Phys. **32**, 453 (1983).
[55] M. Jarrell and O. Biham, Phys. Rev. Lett. **63**, 2504 (1989).
[56] R. N. Silver, J. E. Gubernatis, D. S. Sivia, and M. Jarrell, Phys. Rev. Lett. **65**, 496 (1990).
[57] K. G. Wilson, Rev. Mod. Phys. **47**, 773 (1975).
[58] S. Hershfield, J. H. Davies, and J. W. Wilkins, Phys. Rev. Lett. **67**, 3720 (1991).
[59] A. L. Yeyati, A. Martin-Rodero, and F. Flores, Phys. Rev. Lett. **71**, 2991 (1993).
[60] P. Coleman, Phys. Rev. B **29**, 3035 (1984).
[61] N. S. Wingreen and Y. Meir, Phys. Rev. B **49**, 11040 (1994).
[62] Y. Meir, N. S. Wingreen, and P. A. Lee, Phys. Rev. Lett. **70**, 2601 (1993).
[63] B. Dong and X. L. Lei, J. Phys.: Condens. Matter **13**, 9245 (2001).
[64] J. Paaske, A. Rosch, and P. Wölfle, Phys. Rev. B **69**, 155330 (2004).
[65] A. Schiller and S. Hershfield, Phys. Rev. B **51**, 12896 (1995).
[66] R. M. Konik, H. Saleur, and A. W. W. Ludwig, Phys. Rev. Lett. **87**, 236801 (2001).
[67] X. Wang, C. D. Spataru, M. S. Hybertsen, and A. J. Millis, Phys. Rev. B **77**, 045119 (2008).
[68] F. D. M. Haldane, Phys. Rev. Lett. **40**, 416 (1978).
[69] J. A. White, Phys. Rev. B **45**, 1100 (1992).
[70] B. Holm and U. von Barth, Phys. Rev. B **57**, 2108 (1998).
[71] Value taken from the NIST Chemistry WebBook, http://webbook.nist.gov/chemistry/
[72] F. Guinea, C. Tejedor, F. Flores, and E. Louis, Phys. Rev. B **28**, 4397 (1983).
[73] W. H. Press, B. P. Flannery, S. A. Teukolsky, and W. T. Vetterling, *Numerical Recipes in C: The Art of Scientific Computing* (Cambridge University Press, Cambridge, England, 2007).
[74] We used the DACAPO plane-wave (Ref. 48) code with Vanderbilt ultrasoft pseudopotentials. The unit cell for benzene was 16 Å in each direction, the plane wave cutoff was 340 eV, and we used the PBE xc functional.